

CHARACTERIZING THE WEATHERING OF MASONRY SANDSTONE

by

JOANNA HELEN WILFORD

(Under the Direction of Samuel E. Swanson)

ABSTRACT

Sandstone is commonly used in masonry because of its ease of carving, quarrying, and durability. The purpose of this study is to characterize the mineralogy of masonry sandstone from the quarries used to build the Angkor temples of Cambodia, the iconic “brownstone” buildings of the northeastern United States, and the pre-1906 campus buildings of Stanford University, and relate this mineralogy to the weathering of the sandstone. Samples were examined by thin section petrography, X-ray diffraction, and electron microprobe analysis to identify the composition of the sandstone matrix and cement. X-ray diffraction of the clay fraction proved most helpful at characterizing weathering. Mixed chlorite-smectite was found in the Kulen Mountain, Cambodia sandstone and Portland, Connecticut brownstone. The Stanford sandstone contained mixed illite-smectite. Smectite is highly susceptible to swelling. The presence of swelling clays in the sandstone matrix contributes to damage in the built environment through constant wetting and drying.

INDEX WORDS: sandstone weathering, masonry preservation, clay mineralogy

CHARACTERIZING THE WEATHERING OF MASONRY SANDSTONE

by

JOANNA HELEN WILFORD

B.S., University of Connecticut, 2012

A Thesis Submitted to the Graduate Faculty of The University of Georgia in Partial Fulfillment
of the Requirements for the Degree

MASTER OF SCIENCE

ATHENS, GEORGIA

2015

© 2015

Joanna Helen Wilford

All Rights Reserved

CHARACTERIZING THE WEATHERING OF MASONRY SANDSTONE

by

JOANNA HELEN WILFORD

Major Professor: Samuel E. Swanson
Committee: Bruce Railsback
Paul Schroeder

Electronic Version Approved:

Julie Coffield
Interim Dean of the Graduate School
The University of Georgia
May 2015

ACKNOWLEDGEMENTS

I am especially grateful to my adviser, Dr. Sam Swanson, for his guidance and patience throughout this process. The help of Chris Fleischer at the UGA Microprobe Lab, Dr. Federico Carò at the Metropolitan Museum of Art, Dr. Laura Jones and Sapna Marfatia at Stanford University, and David Wessel of Architectural Resources Group was invaluable in sample collection, historic building and quarry documentation, and analytical work. I am also thankful to the Geological Society of America, Clay Minerals Society, and Miriam Watts-Wheeler Fund for their generous support of this project.

TABLE OF CONTENTS

	Page
ACKNOWLEDGEMENTS	iv
LIST OF TABLES	vii
LIST OF FIGURES	ix
INTRODUCTION TO ARCHITECTURAL WEATHERING	1
Introduction.....	1
Weathering Features and Terminology.....	2
Building Weathering Mechanisms.....	4
Common Masonry Repairs to Vulnerable Architectural Elements	5
Mineral Weathering	7
BACKGROUND OF STUDY AREAS.....	10
Kulen Mountain Sandstone.....	10
Portland Brownstone.....	17
Stanford Sandstone	24
METHODS	31
Sampling.....	31
Petrographic Analysis	36
X-Ray Diffraction	37
Electron Microprobe Analysis	38
RESULTS	40

Petrographic Analysis	40
X-Ray Diffraction Analysis	44
Electron Microprobe Analysis	55
DISCUSSION AND CONCLUSIONS	83
Weathering of the Masonry Sandstones	84
IMPLICATIONS FOR HISTORIC PRESERVATION	90
Kulen Mountain Sandstone.....	90
Portland Brownstone.....	90
Stanford Sandstone	91
REFERENCES	92

LIST OF TABLES

	Page
Table 1: Sandstone terminology	3
Table 2: Petrology and mineralogy of Kulen Mountain sandstone samples	17
Table 3: Petrology and mineralogy of Portland brownstone samples	23
Table 4: Petrology and mineralogy of Stanford sandstone samples	30
Table 5: Modal data for Kulen Mountain sandstone, Portland brownstone, and Stanford sandstone.....	43
Table 6a: Kulen Mountain sandstone sample 104B clay diffraction pattern peak list	46
Table 6b: Kulen Mountain sandstone sample 109B clay diffraction pattern peak list	47
Table 7a: Portland Formation sample PB7 Soil clay diffraction pattern peak list.....	50
Table 7b: Portland brownstone sample PB2 clay diffraction pattern peak list.....	50
Table 8a: Stanford sandstone sample SU3 clay diffraction pattern peak list	53
Table 8b: Stanford sandstone sample SU1 clay diffraction pattern peak list	53
Table 9: Clay fraction comparison of fresh to weathered samples	55
Table 10: Summary of microprobe results.....	56
Table 11: Potassium feldspar microprobe analyses for Kulen Mountain sandstone	57
Table 12: Plagioclase feldspar microprobe analyses for Kulen Mountain sandstone	58
Table 13: Muscovite microprobe analyses for Kulen Mountain sandstone.....	59
Table 14: Biotite microprobe analyses for Kulen Mountain sandstone.....	60
Table 15: Chlorite microprobe analyses for Kulen Mountain sandstone	61

Table 16: Potassium feldspar microprobe analyses for Portland brownstone	66
Table 17a: Plagioclase feldspar microprobe analyses for Portland brownstone.....	67
Table 17b: Plagioclase feldspar microprobe analyses for Portland brownstone	68
Table 18: Muscovite microprobe analyses for Portland brownstone.....	70
Table 19: Biotite microprobe analyses for Portland brownstone.....	71
Table 20: Chlorite microprobe analyses for Portland brownstone	72
Table 21: Potassium feldspar microprobe analyses for Stanford sandstone.....	76
Table 22a: Plagioclase feldspar microprobe analyses for Stanford sandstone	77
Table 22b: Plagioclase feldspar microprobe analyses for Stanford sandstone	78
Table 23: Muscovite microprobe analysis for Stanford sandstone.....	79
Table 24: Biotite microprobe analyses for Stanford sandstone	80
Table 25: Summary of building weathering features.....	86

LIST OF FIGURES

	Page
Figure 1: Common building weathering features	2
Figure 2: Common methods of masonry repair	6
Figure 3: Geologic map of Cambodia.....	11
Figure 4: Angkor temples of northern Cambodia.....	12
Figure 5: Petrographic classification of Kulen Mountain sandstone	16
Figure 6: Portland brownstone buildings	18
Figure 7: Geologic map of the Hartford Basin	19
Figure 8: Petrographic classification of Portland brownstone.....	22
Figure 9: Geologic map of the San Francisco Bay block	25
Figure 10: Stanford University campus buildings	25
Figure 11: Stanford University campus map	26
Figure 12: Petrographic classification of Stanford sandstone.....	29
Figure 13: Kulen Mountain quarries.....	31
Figure 14: Portland brownstone sample locations	33
Figure 15: Stanford sandstone sample locations.....	35
Figure 16: Map of Stanford sandstone sampling	36
Figure 17: Petrographic classification of all sandstones.....	41
Figure 18: Photomicrographs of all sandstones	42
Figure 19: XRD pattern of Kulen Mountain sandstone clay fraction.....	45

Figure 20: XRD pattern of Portland brownstone clay fraction.....	49
Figure 21: XRD pattern of Stanford sandstone clay fraction	52
Figure 22: Accessory minerals in Kulen Mountain sandstone	63
Figure 23: Kulen Mountain sandstone cement	64
Figure 24: Kulen Mountain sandstone matrix	65
Figure 25: Accessory minerals in Portland brownstone	73
Figure 26: Portland brownstone cement	74
Figure 27: Accessory minerals in Stanford sandstone.....	81
Figure 28: Stanford sandstone cement.....	81
Figure 29: Stanford sandstone matrix.....	82

INTRODUCTION TO ARCHITECTURAL WEATHERING

Introduction

Sandstone may receive less notice than other popular masonry materials like granite and limestone, but its rich variety of colors, ease of carving, and relative durability make it a desirable building material. Because of these qualities, sandstone was used to construct some of the most recognizable monuments over the centuries, from Petra in Jordan to Angkor Wat in Cambodia (Turkington and Paradise, 2005). The bedding of sandstone allows the material to be relatively easily quarried into blocks. This bedding contrasts with the massive, unlayered nature of granite, or the thin, brittle slabs of slate commonly quarried for building stone. Although sandstone is well suited as a building material, its use is not without its challenges.

The decay of sandstone masonry is a complex phenomenon affected by climate, exposure to water, and the orientation of bedding in the structure, amongst many other factors (Doehne and Price, 2010). Several studies classify weathering features of masonry materials specific to one site, quantifying the degree of stone recession, or imposing a series of treatments on stone samples in a laboratory setting (Turkington and Paradise, 2005; André et al., 2008; Wangler and Scherer, 2009; Doehne and Price, 2010; Siedel et al., 2010; André et al., 2011; André et al., 2012). Fewer studies seek to describe the weathering process of untreated stone in the natural environment. Before the sandstone has been quarried or ever reached a building, it has already undergone one complete cycle of weathering, and perhaps several more (Taylor and Eggleton, 2001). The purpose of this study is to characterize the mineralogy of masonry sandstone from the source quarries and relate this mineralogy to the weathering of masonry sandstone in structures.

Weathering Features and Terminology

A multitude of terms are commonly used to describe weathering features associated with sandstone masonry (Fig. 1). Many of these terms refer to the manner in which pieces of stone detach from the main structure, or the physical appearance of the stone. They refer entirely to qualitative descriptions, such as exfoliation or discoloration. See also Table 1 for a description of common sandstone terminology.

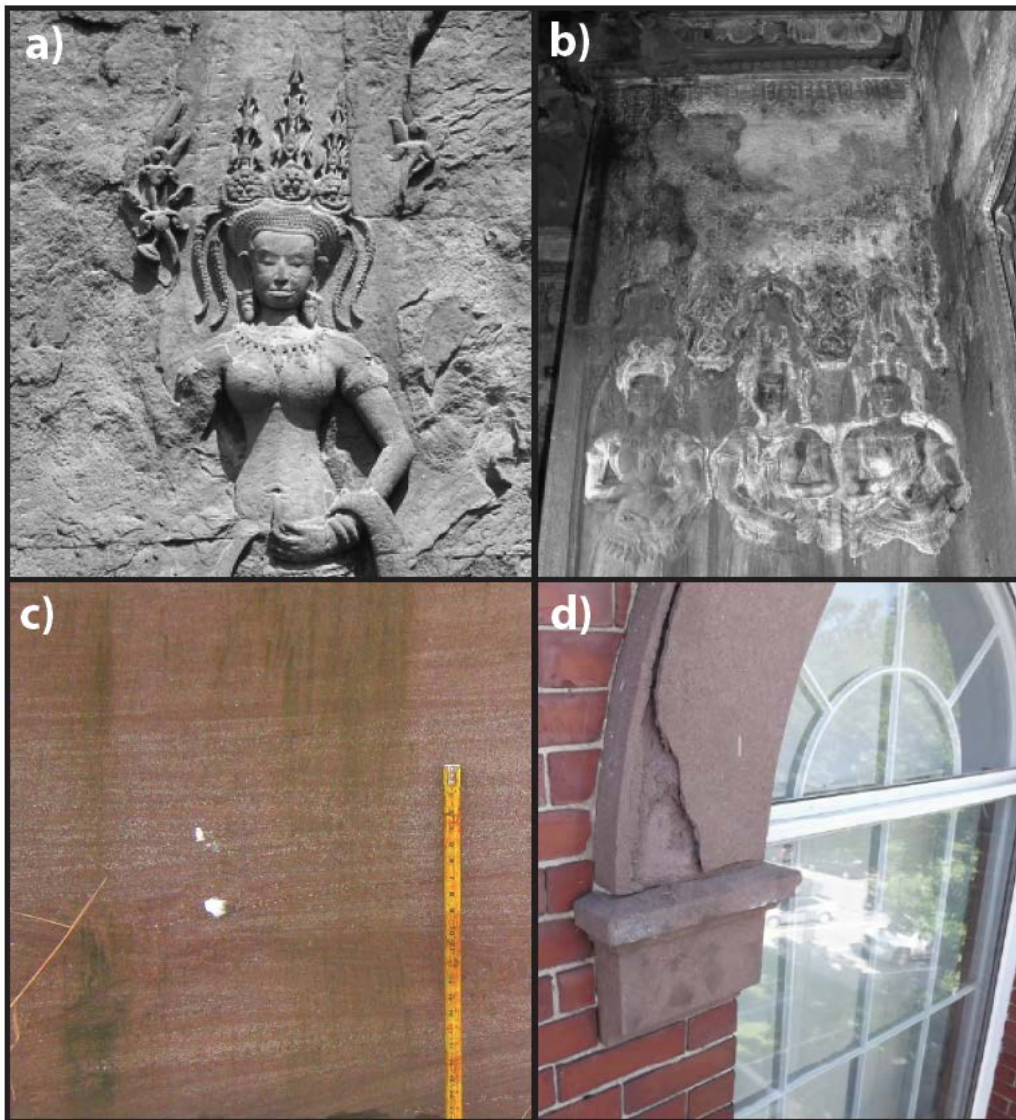


Figure 1. Common building weathering features. (a) Contour scaling and (b) efflorescence at the temple of Angkor Wat as observed by Siedel et al. (2010), (c) biological colonization, and (d) exfoliation of face-bedded Portland brownstone on Concord Townhouse in Concord, MA (image courtesy of Building & Monument Conservation (2012))

Table 1. Sandstone terminology. Definitions modified from the Glossary of Geology (2011).

Term	Definition
Grain	Particle of any size from clay to boulder that composes a sedimentary rock. Sandstone is composed primarily of sand-sized grains, 0.062-2.000 mm in diameter.
Cement	Mineral binding the grains of the sandstone (often chemically precipitated). Mineral cement is most commonly silica, carbonate, and iron oxide. It may also consist of clay, evaporitic, or other detrital minerals.
Matrix	Fine-grained material that fills the space between grains in the sandstone.

Contour scaling/spalling and exfoliation/splitting (Fig. 1a, 1d) involve the loss of large sheet structures from the face of the monument. The difference between the two is the location of the detachment. Contour scaling/spalling occurs at the stone’s surface, but not along the natural bedding plane of the sandstone (Siedel et al., 2010). Exfoliation/splitting occurs along the bedding plane, where the stone comes apart in layers. Face bedding, or laying the natural bedding plane of the stone parallel to the building face, accelerates this type of weathering, and it is particularly noticeable along “slender construction elements like door jambs, columns or pillars” (Siedel et al., 2010; Jiménez González et al., 2012). Flaking can be described as the same as contour scaling, but with much smaller pieces of detached sheets. Similar to flaking, other small-scale weathering forms have been described as blistering and cracking (André et al., 2008).

More weathering terminology describes surface discoloration or the development of a weathered crust changing the appearance of the sandstone (Fig. 1b, 1c). Salt efflorescence describes a crusty layer of minerals precipitated onto the surface of the stone (Siedel et al., 2010). This surface efflorescence contrasts to cryptoflorescence, where salts crystallize within the pores of the stone (Jiménez González et al., 2012). Another type of crust, called a biofilm, forms from microbiological colonization of the stone surface, often causing dark discoloration on the stone’s surface (Architectural Resources Group, 1988; Siedel et al., 2010). The formation of these crusts can lead to a phenomenon called case hardening, where the crust forming the surface

layer leads to the deceptive appearance of hard stone underneath, when in fact, the area behind the crust has lost cement and decayed to a friable texture (Architectural Resources Group, 1988). A hollow ringing sound when the stone is percussed is an indicator of case hardening.

Building Weathering Mechanisms

Climate largely controls the three main building stone weathering processes: wetting and drying, freezing and thawing, and thermal stress. Wetting-drying cycles cause clay in sandstone to absorb water and expand, and shrink upon drying (Siedel et al., 2010). Over several hundred wet-dry cycles, the swelling and shrinking contributes to the degradation of the sandstone through an increase in tensile stress (Siedel et al., 2010; Jiménez González et al., 2012). Humid climates with fluctuations in diurnal temperature and buildings with poor drainage would be particularly susceptible to experiencing these wetting-drying cycles. The complexity of accounting for non-uniform wetting and cumulative fatigue of these cycles over time makes it extremely difficult to acquire direct quantitative evidence on the link between wetting-drying/swelling-shrinking cycles and the tensile strength of sandstone (Wangler and Scherer, 2009; Jiménez González et al., 2012).

Wetting-drying cycles also lead to deterioration through salt crystallization. Water mobilizes salts, which then crystallize on the stone's surface or within the pore network (Scherer et al., 2001; Hosono et al., 2006; Siedel et al., 2010; Jiménez González et al., 2012; Uchida et al., 2012). Efflorescence, or surface salt crystallization, presents mainly cosmetic concerns. Alternatively, cryptoflorescence, where salts crystallize within the pores of the sandstone, poses much higher risks to the stone. Salt crystallization within the pore network exerts a large stress on a small area, causing failure in tension (Jiménez González et al., 2012). "Pulling" forces cause tension, and failure in tension results when the elongating stress exerted from the crystal growth

exceeds the strength of the sandstone pore network. Some factors increasing the risk of supersaturation, and hence crystallization, include rapid drying, small pores, isolated wet zones in the pore network, and hydrating an anhydrous phase (Jiménez González et al., 2012).

Crystallization stress from ice crystal growth during freeze-thaw cycles also causes deterioration of sandstone (Scherer et al., 2001; Jiménez González et al., 2012). Climates that cycle through above and below freezing temperatures on a daily or weekly basis are prone to damage by freeze-thaw cycles. Places that stay consistently above or below freezing are unlikely to experience this type of damage.

Thermal stress results from changes in temperature. It can cause individual minerals to expand and contract at different rates (Scherer et al., 2001; Hale and Shakoor, 2003). Differential stress related to heating can also occur between the exterior and interior of the stone, or between the stone and mortar (Scherer et al., 2001). Maximum temperature is not the key factor in this case, but rather the difference between maximum and minimum daily temperature (André et al., 2012).

Common Masonry Repairs to Vulnerable Architectural Elements

Water is ultimately the cause of many issues related to masonry deterioration. Areas of structures subjected to wetting are the most vulnerable to weathering, and include column bases, features located near drainage spouts, and platform surfaces. Effective treatments attempt to control the movement of water throughout the stone either by physical or chemical means, and sometimes both. Some considerations before deciding on a course of treatment are the presence or absence of mortar, the composition of the mortar (if applicable), the porosity, mineralogy of the stone, and any history of previous treatment of the stone.

At the largest scale, drainage and irrigation can be directed away from the building or monument. On the building scale, grout injection into cavities can prevent water leaching into the building and fortify against cracking. Cement-based patches also repair small surface defects (Fig. 2). More extensive repairs may require a Dutchman. As shown in Figure 2, a Dutchman is a complete or partial replacement of a deteriorated piece of stone with fresh stone designed to match the original stone as closely as possible. Other techniques include preventative chemical treatments. Swelling inhibitors are polymers designed to exchange cations with clay in the sandstone, creating a hydrophobic layer that reduces swelling in the presence of water (Wangler and Scherer, 2009). Additionally, biocides prevent the growth of microbial crusts that hold water on the surface of the sandstone (Jiménez González et al., 2012).

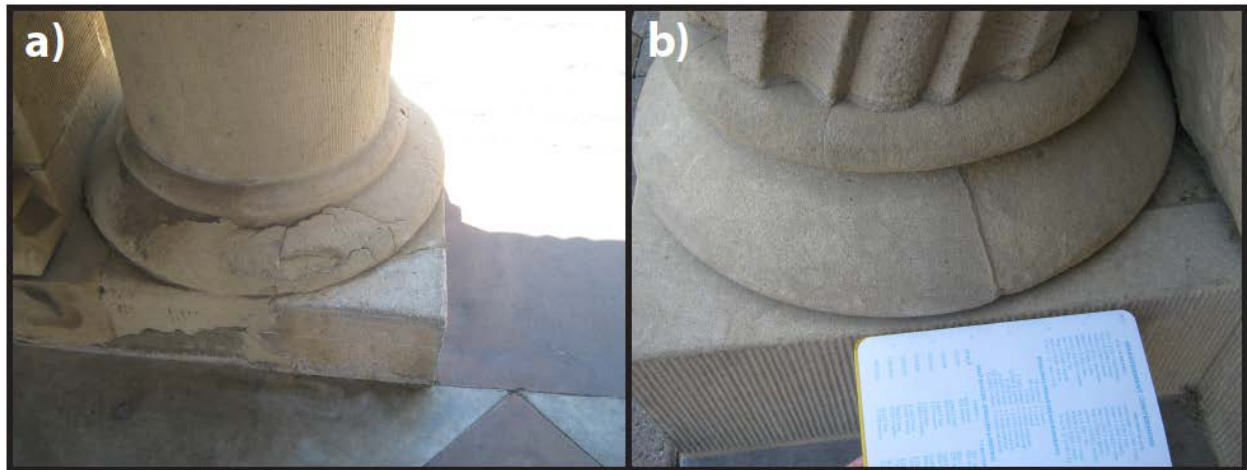


Figure 2. Common methods of masonry repair. (a) Failed patch in Memorial Court, Stanford University, and (b) Dutchman repair on Memorial Church column base.

Mineral Weathering

Quartz

Quartz is the most resistant phase to weathering present in sandstone (Taylor and Eggleton, 2001). The amount of quartz plays a large part in determining sandstone maturity. Quartz arenite is the most mature sandstone, and is comprised of 95% or more quartz, less than 5% matrix, is well-sorted, and contains rounded grains (Blatt and Tracy, 1996). In other words, sandstone is more mature if it contains stable minerals.

Feldspars

Alkali Feldspar

Alkali feldspar is more resistant than plagioclase to weathering (Banfield and Eggleton, 1990). Alkali feldspar first develops etch pits, followed by the crystallization of secondary alteration products. These secondary alteration products develop relatively late in comparison to plagioclase feldspar and mica. Smectite, kaolinite, and halloysite develop from alkali feldspar weathering, with kaolinite being the most abundant alteration product (Banfield and Eggleton, 1990).

Plagioclase Feldspar

Plagioclase weathers more readily than quartz, alkali feldspar, or muscovite (Banfield and Eggleton, 1990). Alteration products appear to develop sequentially. After the formation of the first protocrystalline material, smectite forms. Smectite is a group of 2:1 clay minerals. Montmorillonite, a common smectite mineral, has the general formula $(Al_{1.67}Mg_{0.33})Si_4O_{10}(OH)_2 \cdot nH_2O$ (Moore and Reynolds, 1997). The smectite is richer in calcium, sodium, potassium, and iron than the original feldspar (Banfield and Eggleton, 1990). Further weathering shows the formation of collapsed smectite, halloysite (an expandable 1:1 clay

mineral in the kaolin group), and finally the development of kaolinite (Banfield and Eggleton, 1990; Moore and Reynolds, 1997).

Micas

Muscovite

Muscovite is less susceptible to weathering than feldspars or biotite (Banfield and Eggleton, 1990). The first step in muscovite weathering is the loss of interlayer potassium. Following the loss of potassium, randomly interstratified illite-smectite layers began to replace layers in the muscovite structure. These illite-smectite layers contained much less potassium than unaltered muscovite, and small quantities of magnesium and iron. The appearance of magnesium and iron in muscovite during weathering can occur if biotite is altering nearby. Eventually the illite-smectite alters to kaolinite as the final step (Banfield and Eggleton, 1990).

Biotite

Biotite weathers more easily than quartz, muscovite, and alkali feldspars. Like with muscovite, the first step in the weathering process is the loss of the interlayer cation, potassium (Bisdom et al., 1982; Banfield and Eggleton, 1990). From there, cation exchange occurs and biotite interstratified with either vermiculite or smectite forms (Bisdom et al., 1982). Once all potassium is exchanged, the alteration product becomes entirely vermiculite or entirely smectite. Moore and Reynolds (1997) suggest that vermiculite and smectite should be viewed as a gradient, with vermiculite having a higher layer charge ($z \sim 0.6-0.9$) than smectite ($z \sim 0.2-0.6$).

Chlorite

Chlorite weathering most often is described along the pathway of chlorite, to mixed chlorite-vermiculite, and finally to vermiculite (Taylor and Eggleton, 2001). However, in conditions with poor drainage, some suggest that chlorite weathers to smectite through partial

dissolution and reprecipitation (Istok and Harward, 1982; Buurman et al., 1988). Although much research has been done on chlorite weathering, it is still unknown whether there is a continuous pathway from chlorite to smectite (Moore and Reynolds, 1997).

Cement

Well-cemented sandstones are more resistant to weathering than poorly cemented sandstones. The most common cements in sandstone are calcite, quartz, ferruginous cements (hematite, goethite), and clay minerals (Blatt and Tracy, 1996; Adamovic, 2005). Calcite and quartz chemically weather by dissolution. Calcite readily dissolves at earth surface temperatures and low pH. Quartz requires higher pH and temperature than calcite to favor dissolution, and so is more resistant to weathering (Adamovic, 2005). Ferruginous cements indicate oxidation and the presence of ferric iron. They tend to strongly affect the coloration of sandstone, but do not usually significantly reduce permeability (Adamovic, 2005). The clay minerals kaolinite, smectite, and illite can coat grains and act as cement. Clay mineral cement also weathers through dissolution and reprecipitation (Blatt and Tracy, 1996).

BACKGROUND OF STUDY AREAS

The three sandstones studied in this thesis are from the quarries used to build the temples of Angkor, Cambodia; the iconic “brownstone” buildings of the northeastern United States; and the pre-1906 campus buildings at Stanford University in California. On a broad scale, all of the sandstones are classified as feldspathic arenites (Dott, 1964). Sandstones of this study occur in three different climates and the ages of their structures vary. The Angkor temples are approximately a thousand years older than the nineteenth century brownstone buildings and Stanford University campus buildings. Both the Angkor temples and brownstone buildings are located in a humid climate, in comparison to the semiarid climate of Stanford University. These sandstones were chosen because they were used in historically significant buildings and monuments with severe masonry deterioration problems.

Kulen Mountain Sandstone

Kulen Mountain sandstone is a grey feldspathic arenite used to construct the ninth to thirteenth century Angkor temple complex of humid, tropical northern Cambodia. The sandstone sources from the Kulen Mountain quarrying district, approximately 50 kilometers to the northeast of the Angkor temples. Figure 3 shows the site of the Angkor temples in relation to the Jurassic-Cretaceous sedimentary units of the Kulen Mountain quarrying district.

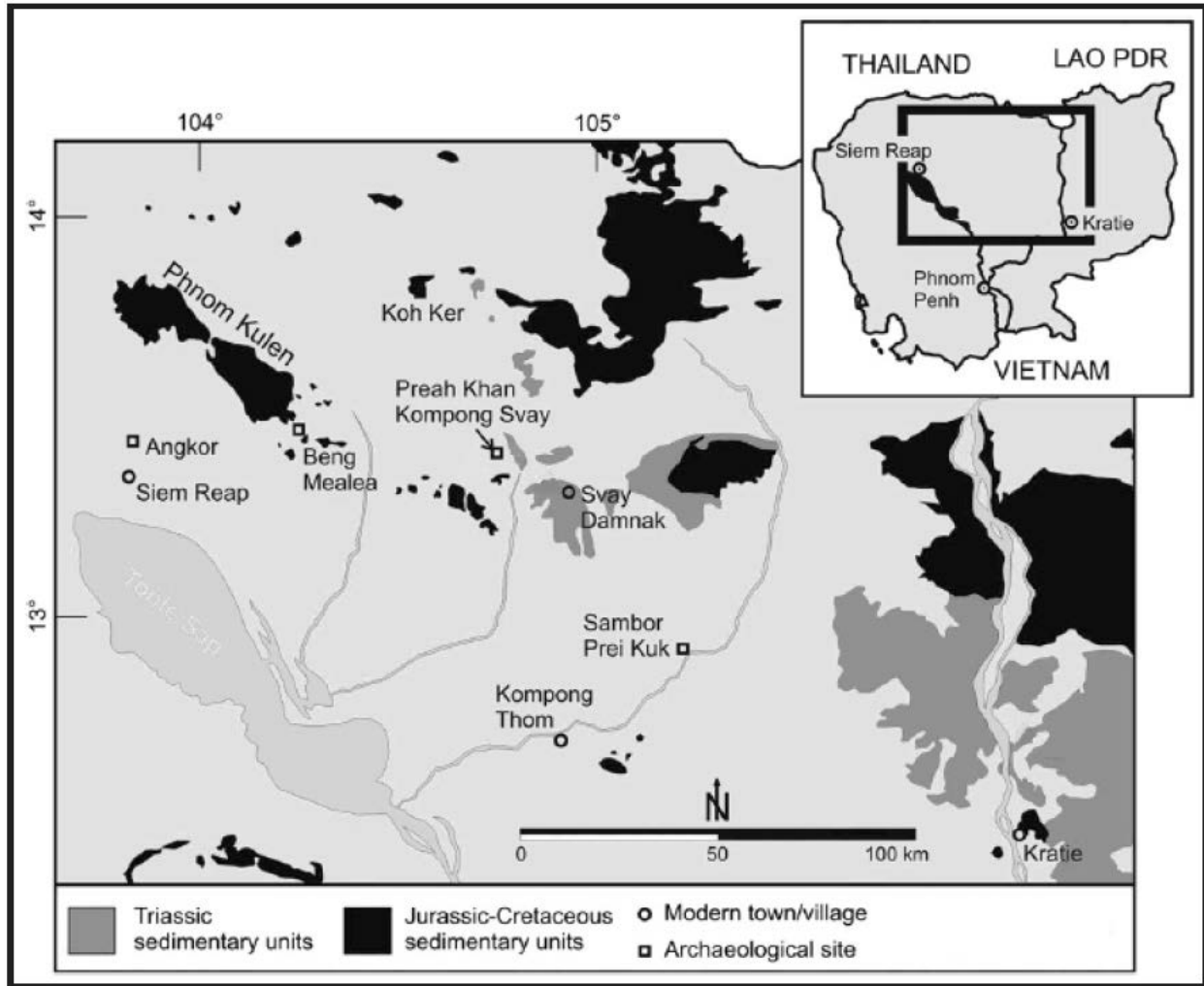


Figure 3. Geologic map of Cambodia after Carò and Douglas (2013) showing the Angkor temples (Archaeological sites) and Kulen Mountain quarrying district. Quaternary units cover the areas surrounding the highlighted Triassic and Jurassic-Cretaceous sedimentary units.

Historic Setting

The sandstone temples and monuments of Angkor, located in northern Cambodia, remain the most recognizable and enduring symbols of Cambodian history and culture (Fig. 4). In the Hindu tradition, the ruler is considered divine and his status celebrated through the construction of a “temple mountain” (Dagens, 2002). An extensive building tradition started with the reign of Jayavarman II (c.800-850 AD) and continued until the end of Jayavarman VII’s reign in 1218 AD. Following Jayavarman VII’s death, Angkor declined and little construction occurred outside of renovations to existing structures until the site was abandoned early in the 15th century (Dagens, 2002).



Figure 4. The Angkor temples of northern Cambodia. (a) the temple of Angkor Wat, (b) Churning Sea of Milk bas-relief, (c) a bas-relief at the temple of Preah Khan, and (d) the temple of Preah Khan. (images courtesy of World Monuments Fund)

Angkor faded into Cambodian history until the ruins captured the attention of French naturalist Henri Mouhot in the 1850s. At the time, France desired access to the Mekong River, and in 1864 Cambodia became a protectorate of France. From 1866 to 1868 two French naval officers, Doudart de Lagre and Louis Delaporte, mapped the Angkor area and collected artifacts for exportation to Paris (French, 1999). It was not until the creation of the École Française d'Extrême Orient (EFEO) in 1898 that preservation factored into the management of Angkor cultural resources (French, 1999). The EFEO recognized the contextual value of sculptures and carvings in situ, and conducted extensive preservation work with French-educated Cambodian conservators. This work continued through the time of Cambodia's independence from France in 1954, until the Khmer Rouge came into power in 1975 (French, 1999).

Civil war filled the intervening years between the Khmer Rouge's deposition in 1979 and a peace agreement in 1991. During that time, the Angkor temples again fell into neglect. The World Monuments Fund (WMF) conducted an assessment of their condition in 1989, spurring the extensive international involvement that continues today (French, 1999).

With international attention fixed on Angkor, a renewed line of inquiry has surfaced on the source of the sandstone for these monuments. Recently, evidence of quarried outcrops and the remains of sculpture workshops have been documented to the northeast of Angkor near Kulen Mountain and Koh Ker (Carò and IM, 2012), and to the southeast of Angkor in the Preah Vihear and Kratie provinces (Carò and Douglas, 2013). The majority of these sites are small and widely scattered, sometimes bearing only a few chisel marks to identify it as a former quarry (Carò and Douglas, 2013). Kulen Mountain and Koh Ker areas show the most extensive evidence of quarrying found to date, with unfinished statues, partially dressed blocks, and stepped surfaces from cut blocks. Even so, quarried outcrops tend to be shallow and surrounded

by heavy vegetation. Several more quarries remain to be discovered to account for the volume of material used to construct the Angkor temples.

Climate and Previous Weathering Studies

Cambodia's tropical monsoon climate contributes to the weathering of temples and monuments, particularly those exposed by deforestation. Both forested and deforested sites experience changes in humidity and temperature between the "rainy" and "dry" seasons in this type of climate. Rainy season runs from May to November, with dry season running from December to April. Of the 1320 millimeters in average annual rainfall, roughly 1162 millimeters falls during the rainy season (André et al., 2012). Overall, average temperature and relative humidity are higher during the rainy season than in the dry season, but more telling than the seasonal variation is the diurnal variation between the two types of sites. Daily temperatures in deforested sites fluctuate widely compared to forested sites because the lack of vegetation exposes the structures to the sun (André et al., 2012). Relative humidity remains slightly higher in forested sites, but varies much less on a daily basis than cleared sites (André et al., 2012).

Several studies describe and attempt to quantify weathering at the temples (André et al., 2008; Siedel et al., 2010; André et al., 2011; André et al., 2012). The studies by André et al. (2008), André et al. (2011, and André et al. (2012) focus on describing the recession of elaborately carved architectural elements. Stone recession depends on the particular sandstone, its position in the temple, and the amount of coverage by vegetation. The degree of recession has been measured through lasergrammetry, and comparison based on a 7-point mechanical weathering and 5-point chemical weathering scale (André et al., 2008; André et al., 2011; André et al., 2012). Another study at Angkor Wat observed that most of the damage on vaults and at the floors of galleries is related to wetting-drying cycles where stone expands when water is

absorbed through capillary action during the rainy season, and shrinks upon drying with exposure to sun and wind in the dry season (Siedel et al., 2010).

Some studies have dealt specifically with testing the salts mobilized from these wetting-drying cycles (Hosono et al., 2006; Uchida et al., 2012). Hosono et al. (2006) identified salts at Angkor Wat, Bayon, Phnom Krom, Phnom Bakheng, and Ta Keo, and then used sulfur and strontium isotopic ratios to determine the source of the salts. They found gypsum present at each temple. In addition to gypsum, calcite occurs on platform surfaces at both Phnom Bakheng and Ta Keo. The calcite is thought to form by leaching from the matrix of the sandstone and reprecipitation on platform surfaces. Other salts (sulfates and phosphates) were thought to come from bat guano (Hosono et al., 2006). Uchida et al. (2012) used non-destructive methods to examine the relationship between water absorption and calcite crystallization on the bas-relief in the inner gallery of Bayon. Aside from a roof collapse exposing the bas-relief to water, the platform behind the bas-relief retains water, mobilizing calcium from the sandstone matrix and reprecipitating as calcite on the surface of the bas-relief (Uchida et al., 2012).

Geologic Setting of Kulen Mountain Sandstone

The majority of Angkor monuments consist of grey sandstone Jurassic to early Cretaceous in age belonging to the Terrain Rouge Formation of Cambodia (Fig. 3) (Delvert, 1963; Carò and IM, 2012). The Terrain Rouge is exposed at the base of Kulen Mountain and around Koh Ker to the northeast of Angkor (Fig. 3), although the majority of outcrops remain isolated and largely unexposed (Carò and IM, 2012). The Terrain Rouge Formation correlates to the Phu Kradung Formation across the Khorat Plateau into Northeast Thailand (Racey et al., 1996; Uchida et al., 2010).

Table 2. Petrology of Kulen Mountain sandstone samples thin-sectioned for this study and mineralogy from Carò and IM (2012).*

Sample	Site	Classification	Cement	Accessory Minerals**	Clay Fraction
104B	Toek Lick	Feldspathic arenite	Chl, Qz	Chl, Ms, Bt, Grt, Ep, Ap, Rt, Ilm, Spn, Mag, Xtm	Chlorite, Chlorite-smectite, Mica-Illite
109B	Toek Lick	Feldspathic arenite	Cal, Ab	Chl, Ms, Bt, Grt, Spn, Ap, Zeo	Chlorite, Chlorite-Smectite, Smectite, Mica-Illite, Calcite

*See results and discussion for additional information on accessory minerals and clay fraction data.

**Mineral abbreviations are as follows: Chl=chlorite, Qz=quartz, Cal=calcite, Ab=albite, Ms=moscovite, Bt=biotite, Grt=garnet, Ep=epidote, Ap=apatite, Rt=rutile, Ilm=ilmenite, Spn=sphene, Mag=magnetite, Xtm=xenotime, Zeo=zeolite.

Portland Brownstone

Portland brownstone is a characteristic red-brown, plagioclase-rich, feldspathic arenite famous in the nineteenth century buildings of Boston, New York City, and Hartford. The sandstone occurs in the Triassic Hartford Basin and is interbedded with shale and conglomerate. It was quarried in the humid temperate climate of Portland, Connecticut.

Historic Setting

The iconic brownstone buildings of the northeastern United States are named for the characteristic chocolate brown sandstone used in their construction (Fig. 6). This brown sandstone is a feldspathic arenite that comes from Portland, Connecticut, on the eastern bank of the Connecticut River just north of Middletown (Fig. 7). Its use was prevalent as a building material in the northeastern United States during the nineteenth century, but was featured in prominent buildings as far away as San Francisco. I used the term brownstone in deference to its widespread use among builders, conservators, architects, and the general public.



Figure 6. Portland brownstone used in (a) rowhouses in Brooklyn, New York and (b) the Pacific Union Club in San Francisco, California. (images courtesy of Brian Harkin (New York Times) and the Library of Congress)

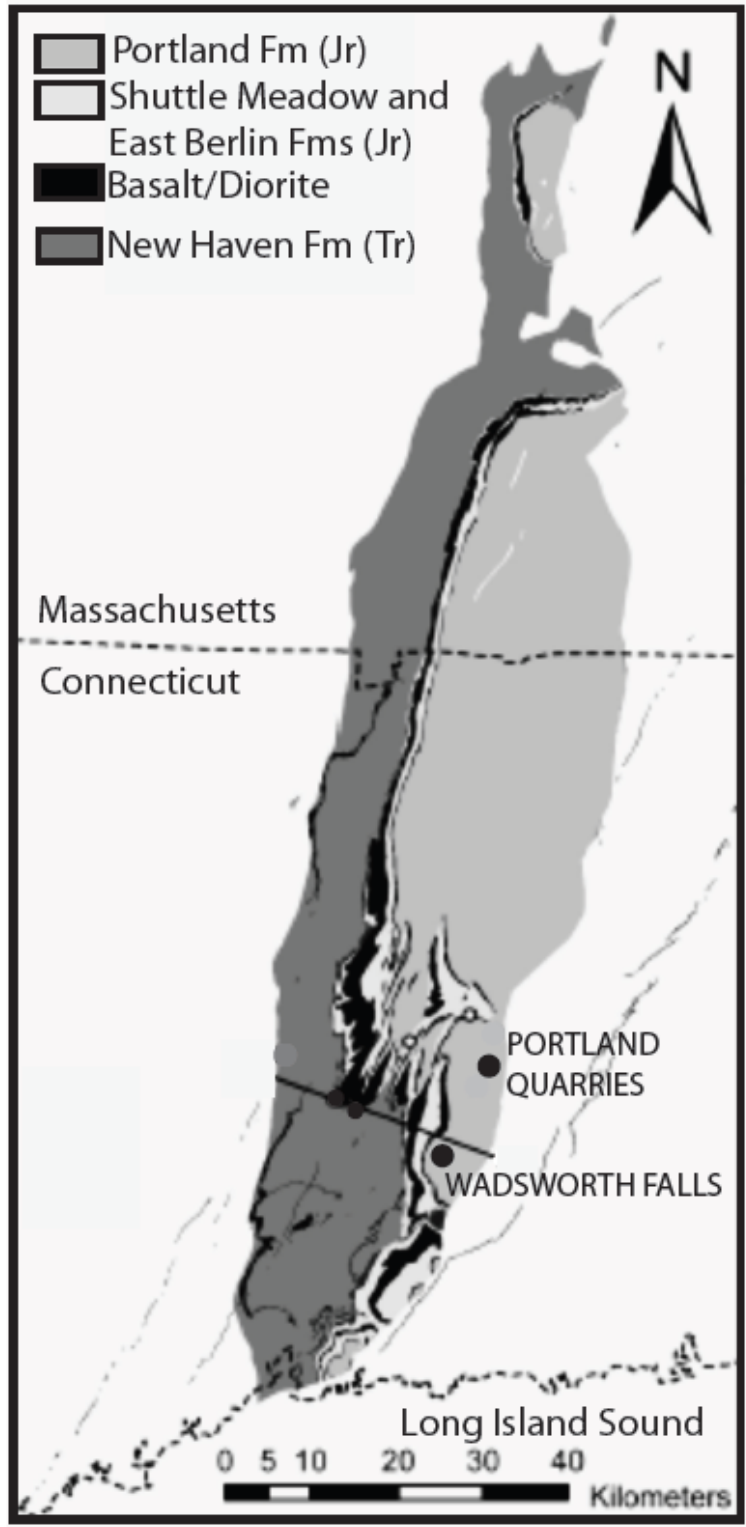


Figure 7. Map of the Portland Formation in the Hartford Basin, Connecticut after Resor and deBoer (2005) showing the source of Portland brownstone.

Brownstone was initially used primarily for gravestones beginning in the mid-1600s and continuing through the late 1700s (Guinness, 2003). The late eighteenth century saw a transition from carving to building stone, and by the mid-1800s several lucrative quarry operations, the Middlesex Quarry Company, Brainerd Quarry Company, Shaler & Hall Quarry Company, and the Town Quarry supplied architectural sandstone. Changes in the economy and fashion in the late 1800s decreased the quarries' production until forcing their final closure after flooding from a 1938 hurricane (Guinness, 2003). In 1993, Michael Meehan reopened a small section of quarry above the flooded site to supply building restoration projects. The last supplier of Portland brownstone, Portland Brownstone Quarries, closed in 2012 (Harris, 2012).

Brownstone proved relatively easy to remove because of its massive, horizontal bedding and perpendicular jointing. Masons extracted blocks along the perpendicular joints using plugs and wedges, and blasted with black powder for more difficult blocks (Guinness, 2003). Modern quarrying operations continued to use the perpendicular joints, but utilized an expansion compound in a series of drilled holes to break apart the rock (Guinness, 2003; Meehan, 2011). After extraction, blocks were left to season, or dry out, for four months, dressed and then shipped along the Connecticut River (Guinness, 2003).

Climate and Previous Weathering Studies

Historically, Portland brownstone was laid with the natural bedding plane of the sandstone parallel to the building face, or "face-bedded", in the buildings in keeping with the fashion of the time. Laying a stone face-bedded contributes to rapid weathering because the stone is weakest along the bedding plane (Guinness, 2003; Jiménez González et al., 2012). With the intentional arrangement of Portland brownstone along its weakest direction, buildings with

brownstone façades began decaying within a couple of decades of their construction (Guinness, 2003).

Freeze-thaw cycles prove a prevalent mechanism of decay in the temperate climate of the northeastern United States, and accelerate the problems caused by face-bedding (Scherer et al., 2001; Wangler and Scherer, 2009; Jiménez González et al., 2012). In addition to freeze-thaw cycles, several studies observed that the migration of soluble salts from mortar, biological colonization, and wetting-drying cycles contributed to the decay of Portland brownstone in this climate (Scherer et al., 2001; Jiménez González et al., 2012).

Most quantitative weathering studies focused on the mechanical properties of Portland brownstone including the elastic modulus; pore size and shape, symmetry, and distribution; and swelling strain (Wangler and Scherer, 2009; Jiménez González et al., 2012). More recent research relates these mechanical properties to stress induced by swelling clays, and to test the effectiveness of consolidants and swelling inhibitors (α,ω -diaminoalkanes) in treating problems produced by these swelling clays (Wangler and Scherer, 2009; Jiménez González et al., 2012).

Geologic Setting of Portland Brownstone

Portland brownstone is part of the Portland Formation of the Hartford Basin in the Newark Supergroup (Fig. 7). The early Jurassic Portland Formation comprises the uppermost 2.2 km of the Newark Supergroup and overlies the Hampden Basalt, East Berlin Formation, Holyoke Basalt, Shuttle Meadow Formation, Talcott Basalt, and New Haven Formation. Sandstones of the Portland, East Berlin, and New Haven Formations collectively group together as “red beds” (April, 1981). The Portland Formation specifically is made up of alluvial sediments deposited at the eastern margin of the half-graben forming the Hartford Basin approximately 220 to 195 million years ago (Hubert et al., 1992).

A variety of clay minerals occur in the brownstone. April (1981) identified 2M illite, chlorite, smectite, and mixed layer illite-smectite, with illite most abundant. Wangler and Scherer (2009) report illite, chlorite, and kaolinite after examining samples solely of architectural Portland brownstone rather than samples from the entire Portland Formation. They attribute the swelling of the stone to randomly distributed swelling layers in the chlorite (Wangler and Scherer, 2009; Jiménez González et al., 2012). Mineralogy of Portland brownstone samples in this study vary slightly from reported clay minerals in the Portland brownstone. See Table 3 for a summary of Portland brownstone mineralogy and the Results Section for a complete discussion.

Table 3. Petrology and mineralogy of Portland brownstone samples thin-sectioned for this study.

Sample	Site	Classification	Cement	Accessory Minerals*	Clay Fraction
PB2	Berkshire Stone, LLC	Feldspathic arenite	Cal, Hem, Ab, Qz	Chl, Mus, Bt, Grt, Rt, Amp, Ilm	Chlorite, Chlorite-Smectite, Mica-Illite
PB6	Berkshire Stone, LLC	Feldspathic arenite	Cal, Hem, Ab, Qz	Chl, Mus, Bt, Grt, Rt, Amp, Ilm, Mag	Chlorite, Chlorite-Smectite, Mica-Illite
PB7	Wadsworth Falls State Park	Feldspathic arenite	Hem, Qz	Chl, Mus, Bt, Amp	Chlorite, Chlorite-Smectite, Mica-Illite
PB7 soil	Wadsworth Falls State Park	n/a	n/a	n/a	Chlorite, Mica-Illite
PB8	Portland, CT	Feldspathic arenite	Hem, Ab, Qz	Chl, Mus, Bt, Grt, Spn, Amp, Ilm	Chlorite, Chlorite-Smectite, Mica-Illite

*Abbreviations as in Table 2, Amp=amphibole, Hem=hematite. See Table 2 for remainder of abbreviations.

Stanford Sandstone

Stanford University is located on the San Francisco Peninsula of central California. Stanford sandstone is a tan feldspathic arenite used to build Stanford University's original nineteenth century campus buildings. The stone comes from Greystone Quarry in the Santa Teresa Hills of California, about 40 kilometers from Stanford. Central California has a semiarid Mediterranean climate. Figure 9 shows the location of Greystone Quarry in relation to Stanford University.

Historic Setting

Leland and Jane Stanford founded Stanford University in 1891 to commemorate their son after his untimely death. Planning began in 1886 under the principal architect Charles Coolidge and landscape architect Frederick Law Olmsted (Architectural Resources Group, 1988; Junkerman, 2010). Construction continued until the 1906 San Francisco earthquake, after which some structures were not rebuilt, and others were reconstructed out of cast concrete rather than sandstone to better withstand future seismic stresses (Joncas et al., 2006; Junkerman, 2010).

The Main Quadrangle (Quad) of Stanford University is a famous example of Mediterranean Romanesque architecture (Fig. 10). The Inner and Outer Quad, Memorial Church, and Memorial Arch comprise the Main Quad, and constitute the original pre-1906 complex of campus buildings (Fig. 11). These buildings are constructed with a tan feldspathic arenite quarried from Greystone Quarry (formerly Goodrich Quarry) just south of San Jose (Fig. 9)(Architectural Resources Group, 1988).

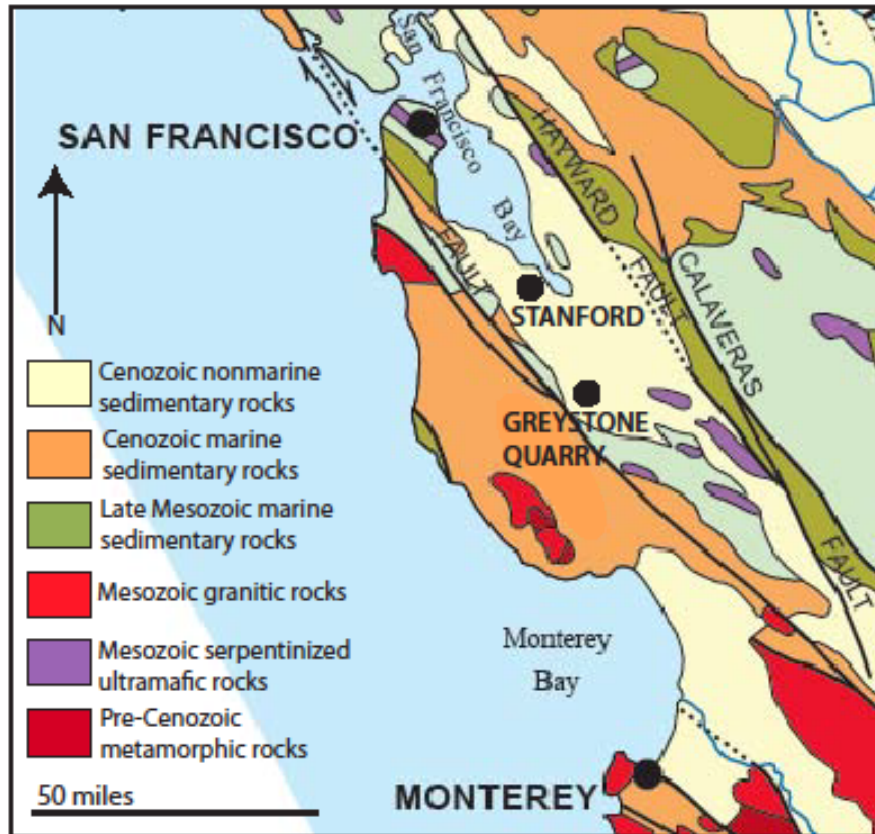


Figure 9. Geologic map (after California Geological Survey, 2006) showing Stanford University and the source of the Stanford sandstone, Greystone Quarry.

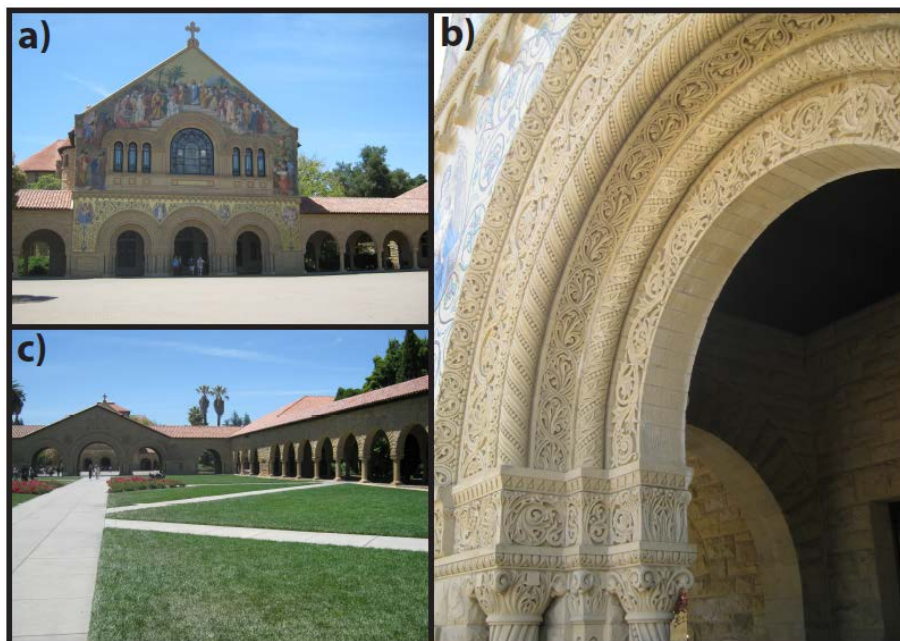


Figure 10. Stanford sandstone used in the construction and detailed carvings of Memorial Church ((a) and (b)) and (c) Memorial Court of Stanford University in California.

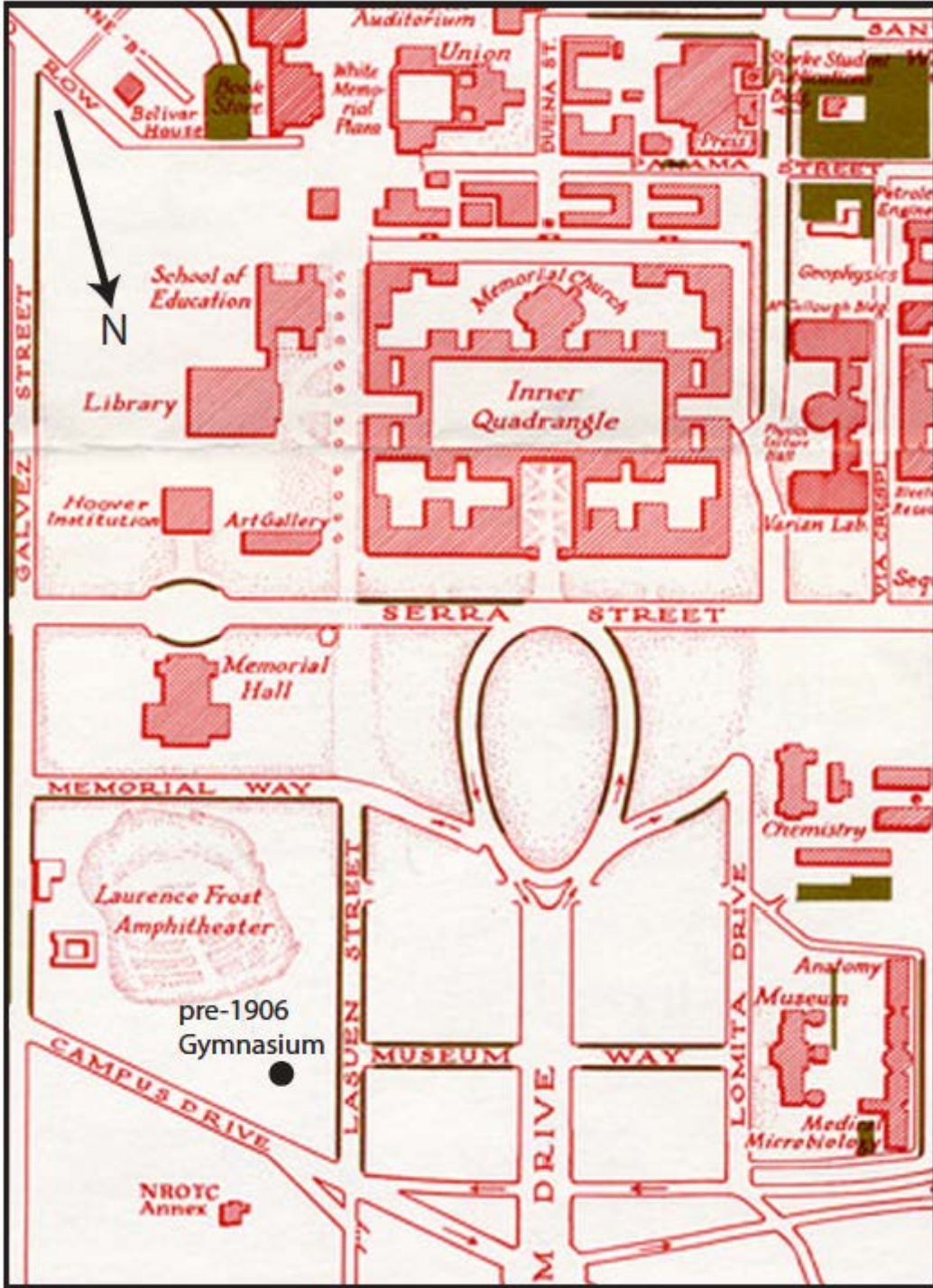


Figure 11. Map of Stanford University campus showing the Main Quadrangle and location of pre-1906 earthquake campus buildings. (image modified from the Stanford University Campus Map ca. 1965)

Climate and Previous Weathering Studies

Stanford has a semiarid Mediterranean climate with a few intense rain events throughout a cool winter, and a dry, temperate summer (Joncas et al., 2006; Camarasa-Belmonte and Soriano, 2014). A weathering study of sandstone from a similar Mediterranean climate in Salamanca, Spain, found that the weathering occurs primarily in areas with poor drainage and is characterized by salt mobilization and efflorescence. The remainder of the sandstone with adequate drainage exhibits little to no damage from physical or chemical processes (Brufau and Vicente, 1986).

No studies have been published regarding the weathering of Stanford University's sandstone. Stanford University Architect, Sapna Marfatia, contracted architectural conservator David Wessel from the private consulting firm Architectural Resources Group to document existing conditions and define a plan for remediation (Architectural Resources Group, 1988). An appendix to the 1988 report contained a petrographic study of sandstone samples from buildings in the Main Quad. Deterioration was noted at places exposed to water (drainage and irrigation systems) and undergoing wetting-drying cycles. Other observed conditions include: case hardening at the stone's surface, spalling at column bases from incompatible patching materials, cracking due to surface expansion, biological growth discoloration, and oxidation discoloration. Of particular concern are the decorative columns in front of Memorial Church, because of their visibility to visitors. Recently they have been repaired using partial replacement with fresh sandstone (Dutchman), after a case of highly incompatible patching material caused rapid decay on the column bases. Although the columns have been repaired, the problem has not been resolved (Sapna Marfatia, personal communication, 2014).

Geologic Setting of Stanford Sandstone

Stanford sandstone comes from Eocene-age strata located in the Santa Teresa Hills of California (Fig. 9), formally known as the Loma Chiquita Ridge sandstone, and informally as “Greystone Formation” sandstone (Short, 1986; Architectural Resources Group, 1988; McLaughlin and Clark, 2004; Junkerman, 2010; Sharman et al., 2014b). California is a continental active plate margin with significant tectonic activity. These Eocene strata were deposited as forearc sediments during Cretaceous-Paleogene low angle subduction of oceanic crust associated with the Laramide orogeny (Sharman et al., 2014a). The sediment sources from the denudation of the Sierra Nevada batholiths to the east (Critelli and Nilsen, 1996; Sharman et al., 2014a). More specifically, the Eocene sedimentary strata are a part of the San Francisco Bay block, bordered by the San Andreas Fault system to the southwest and the Hayward and Calaveras faults to the northeast (Sharman et al., 2014a).

Stanford sandstone is a fine to medium-grained feldspathic arenite (Fig. 12) bound by a clay “pseudo cement” matrix containing goethite (Short, 1986; Architectural Resources Group, 1988; McLaughlin and Clark, 2004). The sandstone is weakly cemented by quartz, albite, and hematite. It contains less than five percent mica and accessory minerals, including biotite, muscovite, magnetite, sphene, zircon, and glauconite (Short, 1986; Architectural Resources Group, 1988). An Architectural Resources Group (1988) report analyzed a suite of seven samples of the Stanford sandstone, with one sample of unaltered stone, and six samples of deteriorated stone representative of weathering forms throughout the Main Quad (Architectural Resources Group, 1988). The report found gypsum present as a crust on the surface of the samples (Architectural Resources Group, 1988). Short (1986) examined three samples of “Greystone Formation” sandstone, and did not report gypsum in any samples. Both

Table 4. Petrology and mineralogy of Stanford sandstone thin-sectioned for this study.

Sample	Site	Classification	Cement	Accessory Minerals*	Clay Fraction
SU1	Stanford University	Feldspathic arenite	Gth, Hem, Ab	Bt, Ms, Ap, Zrn, Glt, Rt	Illite-Smectite, Illite, Kaolinite, Goethite
SU3	Boulder Mountain Way	Feldspathic arenite	Gth	Bt, Ms, Zrn, Glt	Illite-Smectite, Illite, Kaolinite, Goethite
SU5	Hill Lane	Feldspathic arenite	Gth, Hem	Bt, Ms, Zrn, Glt	Illite-Smectite, Illite, Kaolinite, Goethite
SU7	Pramukhs Way	Feldspathic arenite	Gth, Ab	Bt, Ms, Zrn	Illite-Smectite, Illite, Kaolinite, Goethite
SU8	Pramukhs Way	Feldspathic arenite	Gth, Hem	Bt, Ms, Zrn, Glt, Spn	Illite-Smectite, Illite, Kaolinite, Goethite

**Abbreviations as in Tables 2 and 3, Gth=goethite, Zrn=zircon, Glt=glauconite. See Tables 2 and 3 for remainder of abbreviations.

METHODS

Sampling

Angkor sandstone

Angkor sandstone samples used in this study belong to the collection of Carò and IM (2012) at the Metropolitan Museum of Art. Six samples (TL 104T, 104M, 104B and TL 109T, 109M, 109B) of Angkor source sandstone were taken from the site of Toek Lick at the southeastern base of Kulen Mountain. Toek Lick is one of the largest quarry sites in the district (Fig. 13), and one of the few locations where stratigraphic sampling was possible, meaning that the samples were taken from the top, middle, and bottom of the quarried outcrop (Carò and IM, 2012). A dark weathered crust was present on all of the samples. Analytical work was limited by the small size of the samples. All samples were chips approximately two centimeters long, two centimeters wide, and one centimeter tall.



Figure 13. (a) Quarried outcrop at the site of Toek Lick in the Kulen Mountain quarrying district of Cambodia, and (b) evidence of chisel marks. (images courtesy of Carò and IM (2012)).

Portland brownstone

Portland brownstone possesses large variation in grain size and sorting. Jimenéz González et al. (2012) categorized the stone into four grades, listed here from most to least desirable in architectural quality: (1) medium-grained, (2) fine-grained with the highest mica and clay content, (3) fine-grained, interbedded with shale, and (4) conglomerate. The medium grained brownstone was most commonly used in buildings. A total of eight samples of Portland brownstone (PB1-PB6, PB8, PB9), one sample of Portland Formation sandstone (PB7), and one soil sample (PB7 Soil) were collected for the purposes of this study. The samples were chosen to be representative of the variation in architectural quality.

The eight Portland brownstone samples originate from Portland Brownstone Quarries, Inc. (Fig. 14a, 14b), which supplied restoration stone, and lies adjacent to the nineteenth and early twentieth century flooded brownstone quarries. Currently, the site of the restoration quarry remains inaccessible. Six of these samples (PB1-PB6) were taken from a large slab of undressed Portland brownstone (Fig.14d) now located at Berkshire Stone, LLC in Winsted, Connecticut. This slab has been weathering in the open for about a decade, and measures approximately 3m x 1.5m x 1m. It contains medium sand cross-bedded with coarse sand and pebbles. Spalling is present on the surface of the slab, along with green staining that most likely is biological colonization. The remaining two samples (PB8 and PB9) are patio stones that come from the private stockpile of Mrs. Pam Geato. Figure 14 shows the various sampling locations for the Portland brownstone.



Figure 14. (a) Perpendicular jointing and (b) the quarry face at Portland Brownstone Quarries, Inc. in Middletown, CT, (c) exposure of Portland Formation sandstone at Wadsworth Falls State Park in Middlefield, CT, and (d) Portland brownstone block at Berkshire Stone, LLC in Winsted, CT sampled in this study.

The original soil above the Portland quarries has been removed and replaced with manmade fill during reclamation. To approximate the weathering profile at the Portland quarries, a sample of Portland Formation sandstone (PB7) and overlying soil was taken from a stream cut at the Little Falls of Wadsworth Falls State Park in Middlefield, Connecticut (Fig. 14c). The sandstone in this location is more thinly bedded than at the Portland quarries, and is interbedded with shale (LeTourneau, 1985). Additionally, the sandstone appears more fine-grained overall than the optimal architectural stone. However, according to LeTourneau (1985), the Portland Formation sandstone at Wadsworth Falls State Park most closely resembles that of the Portland quarries.

Stanford sandstone

Sampling was conducted both at Stanford University and at the former site of Greystone Quarry around San Jose, California. Sampling was done to represent the range of sandstone weathering conditions observed in Stanford University's Main Quad, including case hardening, flaking, and discoloration. Less weathered samples were also included to represent the well-preserved sandstone, such as is present in the intricate carvings of the entry to Memorial Church.

Two samples of the Stanford sandstone come from the collection of University Archaeologist Dr. Laura Jones, who excavated the original Stanford University Men's Gymnasium building that collapsed during the 1906 San Francisco earthquake (Fig. 15). The blocks had been buried until the 2008-2010 excavation, and since that time sitting exposed in a pile. Both samples came from blocks approximately 20 cm x 15 cm x 30 cm with architectural details such as tooling and scrollwork (Fig. 15a). Aside from some minor surface discoloration from burial and likely biological growth, the sandstone appears quite sound and the carved details intact.

The remaining six samples were obtained from a suburb just south of San Jose, California, and the former site of Greystone Quarry (Fig. 15c, 15d), the source of the Stanford sandstone (Figs. 15 and 16). Only a few small road cuts are available to sample, as most of the sandstone outcrops are inaccessible, privately held ranchland. No overlying soil was available for sampling, as the road cuts had only boulders accessible. Overlying soil would give the final alteration products of sandstone weathering. Two samples came from boulders at a roadcut on Boulder Mountain Way (Fig. 15b, Fig. 16), and one from a boulder on Hill Lane (Fig. 16). The last three samples came from fallen rocks at an outcrop of the Stanford sandstone located on

Pramukhs Way (Fig. 16). This outcrop preserves a small portion of the original quarry face of Greystone Quarry, and contains evidence of drill holes.

Although this site is the closest approximation of the original quarry, the majority of the quarry face was altered when the homeowner blasted to remove a large quantity of stone from the property. Additionally, stratigraphic sampling was not possible at this location because of the homeowner's instruction to sample only fallen blocks.

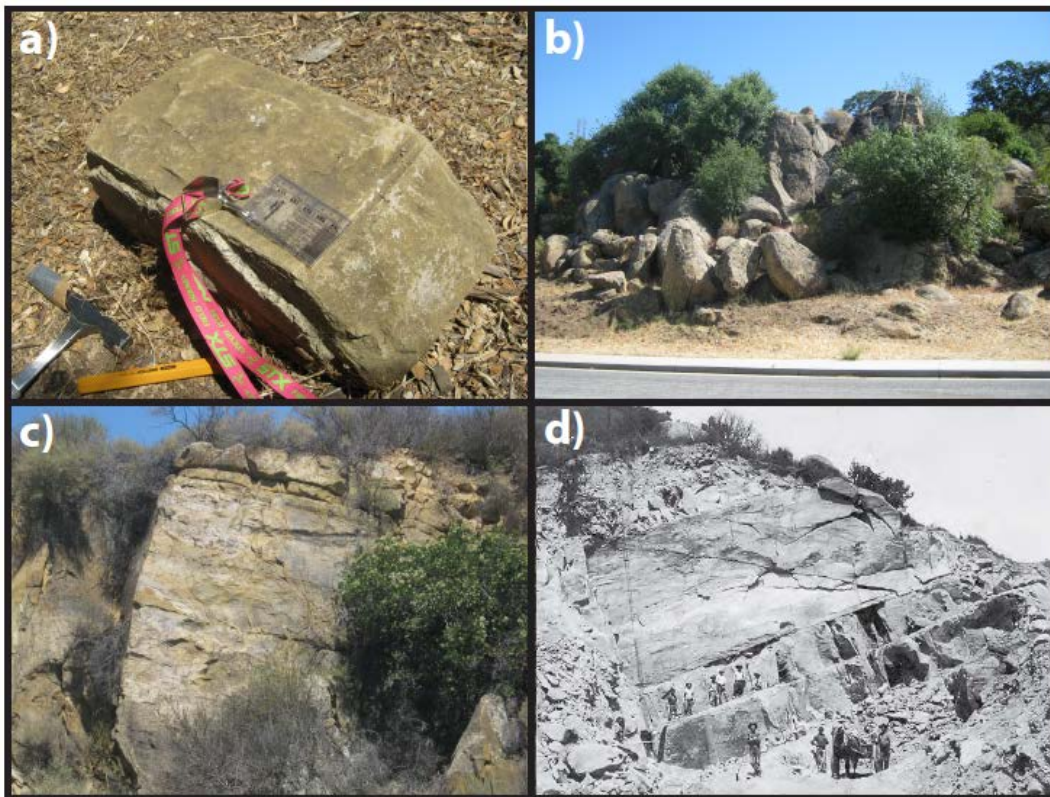


Figure 15. (a) Stanford sandstone block recovered from the former Gymnasium building, (b) boulders sampled from Boulder Mountain Way, (c) site of the former Greystone Quarry on Pramukhs Way, and (d) historic photograph of Greystone Quarry from Junkerman (2010).

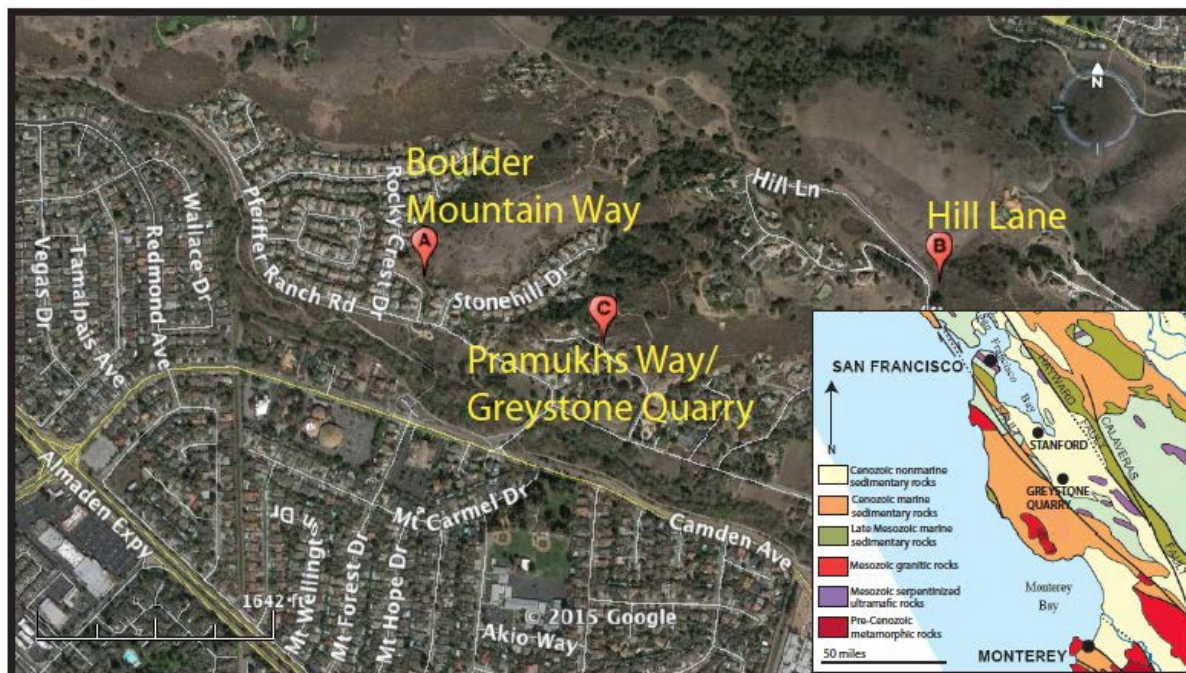


Figure 16. Map showing sample locations of Stanford sandstone near the former site of Greystone Quarry. (a) Boulder Mountain Way, (b) Hill Lane, and (c) Pramukhs Way. (map courtesy of Google Maps)

Petrographic Analysis

Two samples of Kulen Mountain sandstone (TL 104B, TL 109B; Table 1), four samples of Portland brownstone (PB2, PB6, PB7, PB8; Table 2) and five samples of Stanford sandstone (SU1, SU3, SU5, SU7, SU8; Table 3) were selected for thin section analysis. Samples were selected based on size (large enough to cut a thin section), and to represent fresher and more weathered sandstone. Pieces of selected samples were cut to a thickness of one centimeter and fitted to the length and width of a standard 27 mm x 46 mm glass slide. They were sent to Applied Petrographic Services and Vancouver Petrographics for polished thin section preparation, which involves impregnating the slides with epoxy, cutting the blanks to a thickness of 30 μm , polishing the sample, and leaving it uncovered for later use in electron microprobe analysis.

Thin sections were examined under a Leica DM750P polarized light microscope to identify the mineralogy, record grain size and cement of the sandstone, and describe any weathering effects. Modal analysis used 300 points per slide to determine the abundance of quartz, feldspar, lithic fragments, mica, and matrix. Photomicrographs of samples were also taken using a camera mounted to the microscope.

X-Ray Diffraction

X-ray diffraction (XRD) was used to determine the mineralogy of the clay fraction of the sandstone. Six samples of Kulen Mountain sandstone, five samples of Portland brownstone, and six samples of Stanford sandstone were prepared for clay analysis following the Moore and Reynolds Glass Slide Method (Moore and Reynolds, 1997). Approximately 4 grams of hand ground sample combined with sodium hexametaphosphate dispersant and deionized water were agitated with an ultrasonic probe for 1 minute, and then centrifuged for three cycles of two minutes at 2000 rpm. The supernatant containing the clay fraction ($<2\mu\text{m}$) was saturated with 0.1 M potassium chloride (KCl), and centrifuged with deionized water for three cycles of 30 minutes each at 2000 rpm.

The settled clay was pipetted with a small amount of deionized water onto a standard glass petrographic slide and allowed to air dry for 24 hours. Samples were run on the University of Georgia's Bruker D-8 Advance X-Ray Diffractometer equipped with a cobalt X-ray source. The Angkor samples were scanned from 2 to $90^\circ 2\theta$, with a step scan width of 0.01° at a rate of 0.2 seconds per step. These samples needed to be scanned slowly to account for the thinness of the material on the glass slide. The remainder of the samples were scanned 2 to $90^\circ 2\theta$, with a step scan width of 0.01° at a rate of 0.1 seconds per step.

After running in the air-dried state, the slides were then ethylene glycol saturated for 24 hours. They were then run through the XRD again using the same scan parameters as stated above. Movement of the ethylene glycol saturated pattern in comparison to the air-dried pattern indicates the presence of swelling clays.

Electron Microprobe Analysis

Electron microprobe analysis (EMPA) was conducted on a JEOL JXA-8600 Superprobe at the University of Georgia Electron Microprobe Laboratory. Analyses were conducted at an accelerating voltage of 15 kV, beam current of 15 nA, and beam diameter of 10 μm . This analysis used the same polished thin sections used for petrographic analysis.

The microprobe was set up for quantitative analysis on feldspars, micas and chlorites, with four wavelength dispersive spectrometers (WDS), ten second counting times, and mineral standards. Routines analyzed for Si, Ti, Al, Fe, Mn, Mg, Ca, Na, and K. Three to five plagioclase grains from each sample were examined to determine their calcium content. Several mica grains from each sample were also analyzed to determine iron content.

Quantitative analyses of feldspars, micas, and chlorites were selected based on oxide weight percent totals and stoichiometry. Target weight percent totals for feldspars are between 99 and 101, for micas between 94 and 96, and chlorites between 85 and 86. Where possible, analyses with ideal weight percent totals and correct stoichiometry were used, and analyses with weight percent totals below the ideal range discarded. However, due to the weathered nature of the majority of grains, lower totals with correct stoichiometry have been included in the final analysis. Weight percent oxide values below minimum detection limits were removed before calculating formulas.

The microprobe is equipped to conduct qualitative energy dispersive spectroscopy (EDS) with a Bruker Quantax energy dispersive analysis system. EDS was used for mineral identification. The EDS system also allowed rapid collection of data for mapping element distributions.

RESULTS

Petrographic Analysis

Kulen Mountain sandstone

Kulen Mountain sandstone is a fine-grained, moderately well-sorted feldspathic arenite (Fig. 17) cemented with calcite and chlorite (Figs. 18a, 18b) (Carò and IM, 2012). Table 5 shows the modal analysis for the Kulen Mountain sandstone. Feldspar includes both potassium feldspar and poorly-twinned plagioclase. Samples show an abundance of oriented mica. Accessory minerals include garnet, zircon, epidote, muscovite, biotite, chlorite, and opaque phases. The presence of sphene, rutile, and ilmenite among the opaque phases was confirmed with electron microprobe analysis.

Portland brownstone

Portland brownstone is a medium to coarse grained, poorly sorted feldspathic arenite (Fig. 17) cemented by albite, quartz, and calcite, with hematite acting as secondary cement (Figs. 18c, 18d) (Hubert et al., 1992; van de Kamp and Leake, 1996). Table 5 shows the modal analysis for the Portland brownstone. Feldspar includes potassium feldspar and plagioclase. Very fine-grained clay gives the feldspars a “dusty” appearance in comparison to quartz grains. There is an abundance of polycrystalline quartz. Chlorite flakes are abundant and commonly intergrown with hematite. Biotite is extensively weathered. Accessory minerals include muscovite, biotite, garnet, and opaque phases. Microprobe reconnaissance confirmed the presence of apatite, ilmenite, magnetite, amphibole, and zircon.

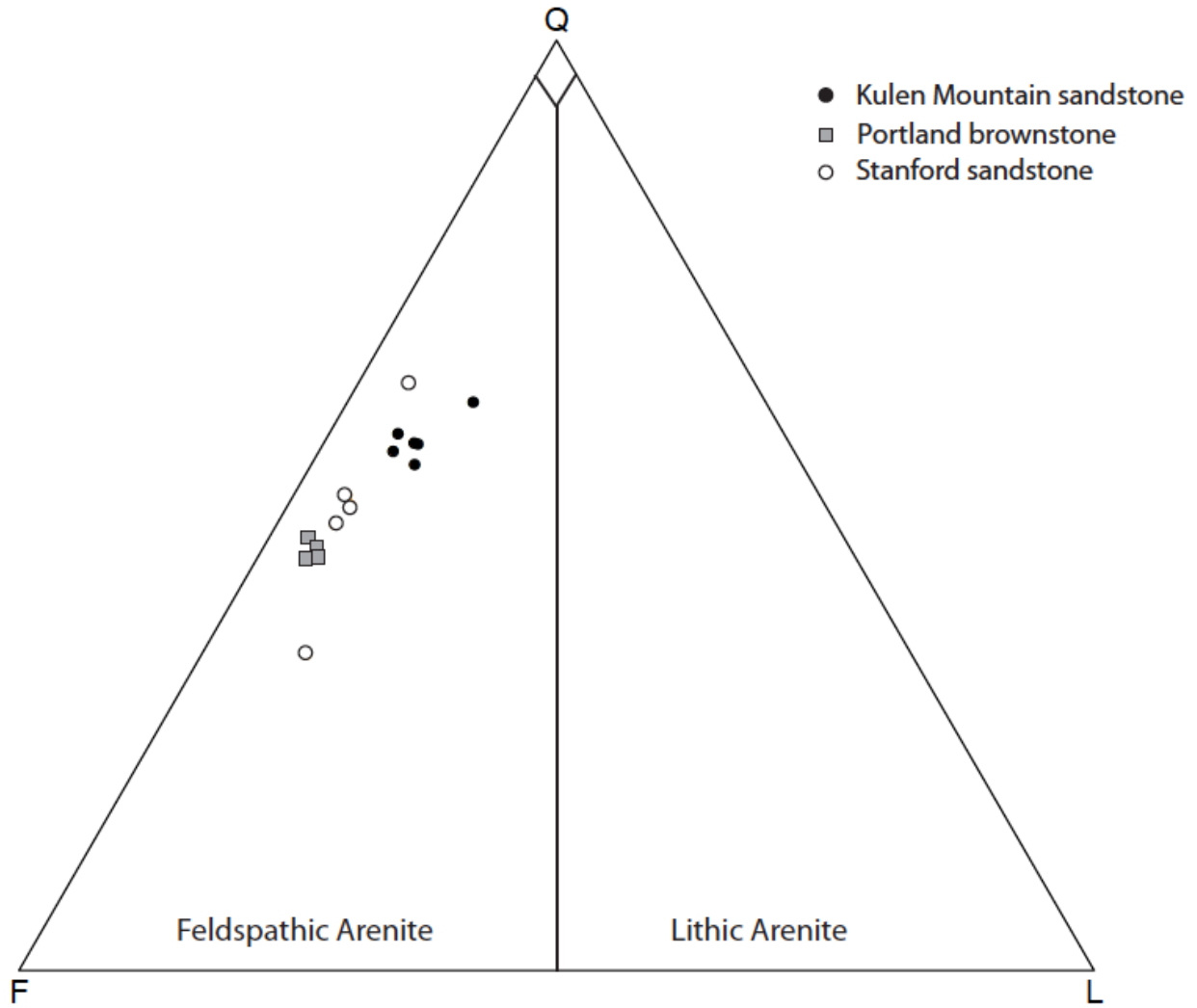


Figure 17. Petrographic classification of Kulen Mountain sandstone (black dots), Portland brownstone (grey squares), and Stanford sandstone (open circles) after Dott (1964). Q=Quartz + Chert, F=Feldspar, L=Lithic fragments.

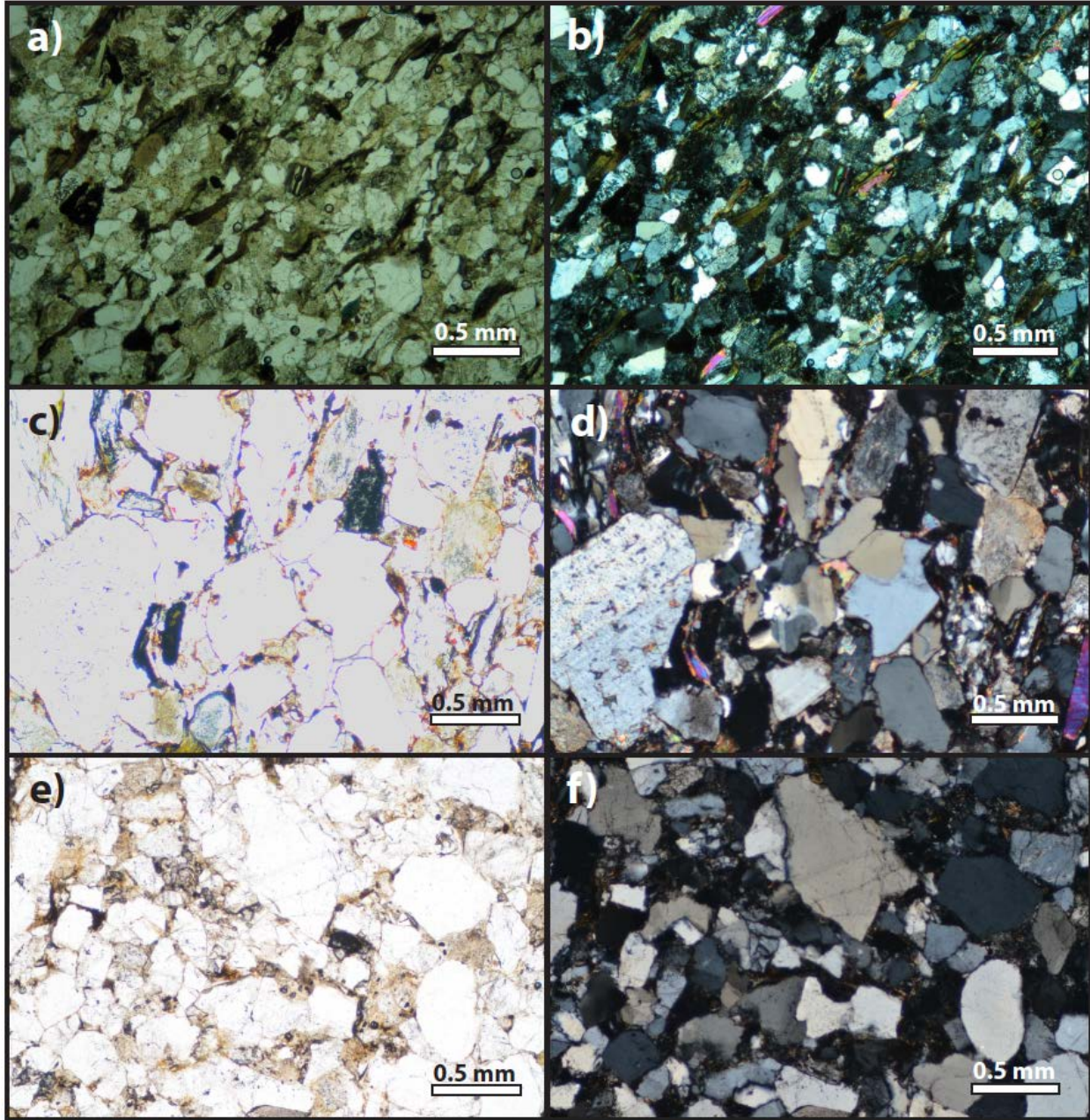


Figure 18. Photomicrographs of the three sandstone types. Sample 104B of Kulen Mountain sandstone under (a) PPL and (b) XPL. Sample PB2 of Portland brownstone under (c) PPL and (d) XPL. Sample SU8 of Stanford sandstone under (e) PPL and (f) XPL.

Table 5. Modal data for Kulen Mountain sandstone, Portland brownstone, and Stanford sandstone.

Kulen Mountain sandstone*

Sample	Q	F	L	Matrix %
104T	56.6	34.6	8.8	5.8
104M	54.4	36	9.6	4
104B	56.7	34.9	8.4	5.5
109T	55.8	37.3	6.9	1.8
109M	57.7	35.9	6.4	1.5
109B	61.1	27.2	11.7	1.8

*Petrography done by Carò and IM (2012)

Portland brownstone

Sample	Q	F	L	Matrix %
PB2	44.4	51.2	4.4	5.3
PB6	46.5	49.8	3.7	6.0
PB7	44.5	50.2	5.3	5.0
PB8	45.4	49.6	5.0	5.0

Stanford sandstone

Sample	Q	F	L	Matrix %
SU1	63.1	32.1	4.7	8.0
SU3	34.0	56.3	9.7	8.0
SU5	48.0	46.6	5.4	6.7
SU7	50.0	44.2	5.8	6.0
SU8	51.1	44.0	4.9	9.3

Stanford sandstone

Stanford sandstone is classified as a fine-grained, moderately well-sorted feldspathic arenite (Fig. 17) weakly cemented with hematite, goethite, and albite (Figs. 18e, 18f). Table 5 shows the modal analysis for the Stanford sandstone. Rare accessory minerals include biotite, muscovite, apatite, zircon, glauconite, and opaque phases. Microprobe analysis confirmed the presence of apatite, sphene, and zircon. The mica phases appear compacted and wrap around grains of quartz and feldspar. Glauconite pellets are strongly colored green in plane light, and exhibit second order interference colors under cross-polarized light.

X-Ray Diffraction Analysis

Six samples of Kulen Mountain sandstone, five samples of Portland brownstone, and six samples of Stanford sandstone were examined using X-ray diffraction. Two representative X-ray patterns from each study area are discussed below.

Kulen Mountain sandstone

The clay fraction of the Kulen Mountain sandstone contains mostly chlorite, with smaller amounts of mixed chlorite-smectite, a mica-illite phase, and residual amounts of quartz and feldspar (Fig. 19). Tables 6a and 6b list diffraction peaks for selected samples of Kulen Mountain sandstone. Movement around 10\AA after ethylene glycol saturation indicates the presence of swelling smectite layers in the chlorite structure, leaving the non-swelling illite-mica phases in place even after EG-saturation. One sample, 109B, contains a larger proportion of smectite layers in the mixed chlorite-smectite. The complete collapse of the peak at 10.8\AA and movement to 27.3\AA upon EG-solvation illustrates the presence of the smectite. Sample 109B is also unique in that it contains a significant amount of calcite in the clay fraction.

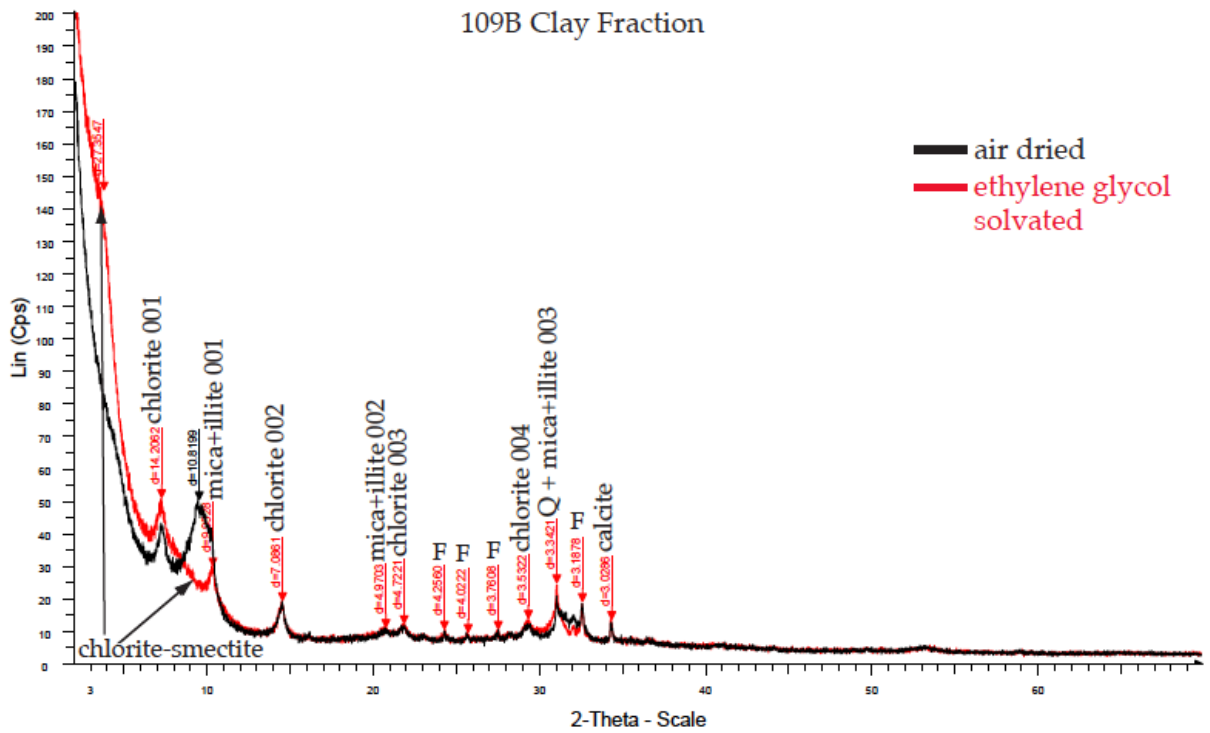
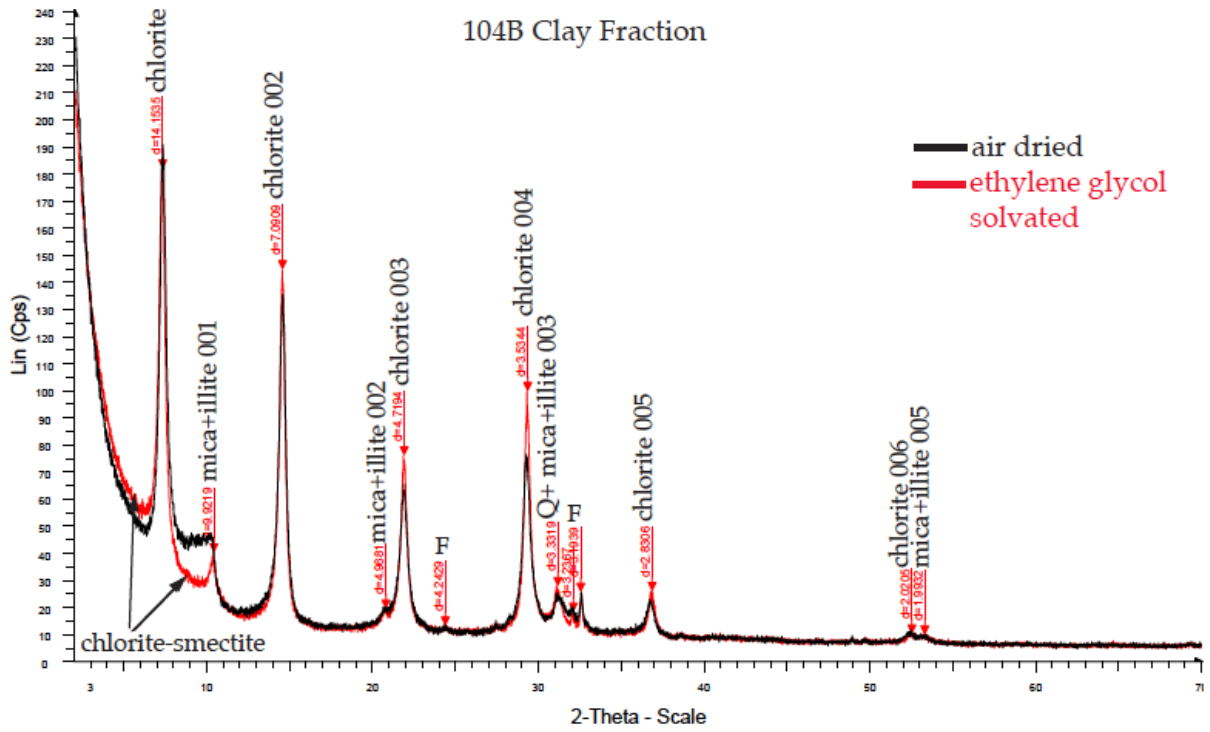


Figure 19. Selected clay fraction diffraction patterns for Kulen Mountain sandstone samples 104B and 109B. The patterns were generated using $Co_{K\alpha}$ radiation.

Table 6a. Kulen Mountain sandstone sample 104B clay diffraction pattern peak list.

Sample 104B Air Dried							
Clay	Order of reflection by d-spacing (Å)						
	(001)	(002)	(003)	(004)	(005)	(006)	(007)
Chlorite/ Chl-Smectite*	14.10	7.09	4.73	3.54	2.84	Absent	2.02
Mica/Illite	9.99	5.00	3.33	Absent	1.99	Absent	1.41
Sample 104B Ethylene Glycol Saturated							
Clay	Order of reflection by d-spacing (Å)						
	(001)	(002)	(003)	(004)	(005)	(006)	(007)
Chlorite/ Chl-Smectite*	14.16	7.08	4.72	3.53	2.83	Absent	2.02
Mica/Illite	9.96	4.96	3.33	Absent	1.99	Absent	1.41

Other minerals identified: Quartz (3.34Å), K-spar (3.24Å), Albite (3.19Å)

*Chlorite-smectite reflections form as the result of two layer types, chlorite and smectite. The asterisk denotes the pair modulated reflection of mixed layered clays, rather than the usual crystallographic *hkl* notation.

Table 6b. Kulen Mountain sandstone sample 109B clay diffraction pattern peak list.

Sample 109B Air Dried								
Clay	Order of reflection by d-spacing (Å)							
	(001)	(002)	(003)	(004)	(005)	(006)	(007)	(008)
Chlorite-Smectite*	23.41	10.90	Absent	6.37	4.24	4.03	3.76	3.02
Chlorite	14.20	7.08	4.72	3.53	Absent	Absent	Absent	Absent
Mica/illite	10.01	5.00	3.33	Absent	1.99	Absent	Absent	Absent
Sample 109B Ethylene Glycol Solvated								
Clay	Order of reflection by d-spacing (Å)							
	(001)	(002)	(003)	(004)	(005)	(006)	(007)	(008)
Chlorite-Smectite*	26.20	Absent	Absent	Absent	4.24	4.02	3.76	3.03
Chlorite	14.20	7.09	4.72	3.54	Absent	Absent	Absent	Absent
Mica/illite	9.97	4.99	3.33	Absent	Absent	Absent	Absent	Absent

Other minerals identified: Quartz (3.34Å), K-spar (3.24Å), Albite (3.18Å)

*See Table 6a for note on chlorite-smectite.

Samples 109M and 109B show lower intensity and lessened sharpness of peaks compared to the remainder of the samples, which indicates a higher proportion of mixed layering and disorder in the clay structure of the mixed chlorite-smectite. In contrast, samples 104T, 104M, 104B, and 109T appear to have a higher proportion of chlorite layers because of high intensity, sharp peaks, and the presence of high order reflections (up to chlorite (006)).

Portland brownstone

Chlorite dominates the clay fraction of all Portland brownstone samples and the Portland Formation soil sample. The intensity of the chlorite peak is illustrated by the selected diffraction patterns for Portland brownstone and Portland Formation soil shown in Figure 20. There is also evidence of a small amount of mixed chlorite-smectite, with movement around 10Å after ethylene glycol saturation in PB2, PB6, PB7, and PB8. A lack of movement with EG-solvation indicates there is no mixed chlorite-smectite in the soil sample. In addition to chlorite and chlorite-smectite, Portland brownstone contains a mica-illite phase, quartz, feldspar, and hematite in the clay fraction. The Portland Formation soil sample also contains mica-illite, quartz, feldspar, and hematite. Tables 7a and 7b list diffraction peaks for selected samples of Portland brownstone and Portland Formation soil.

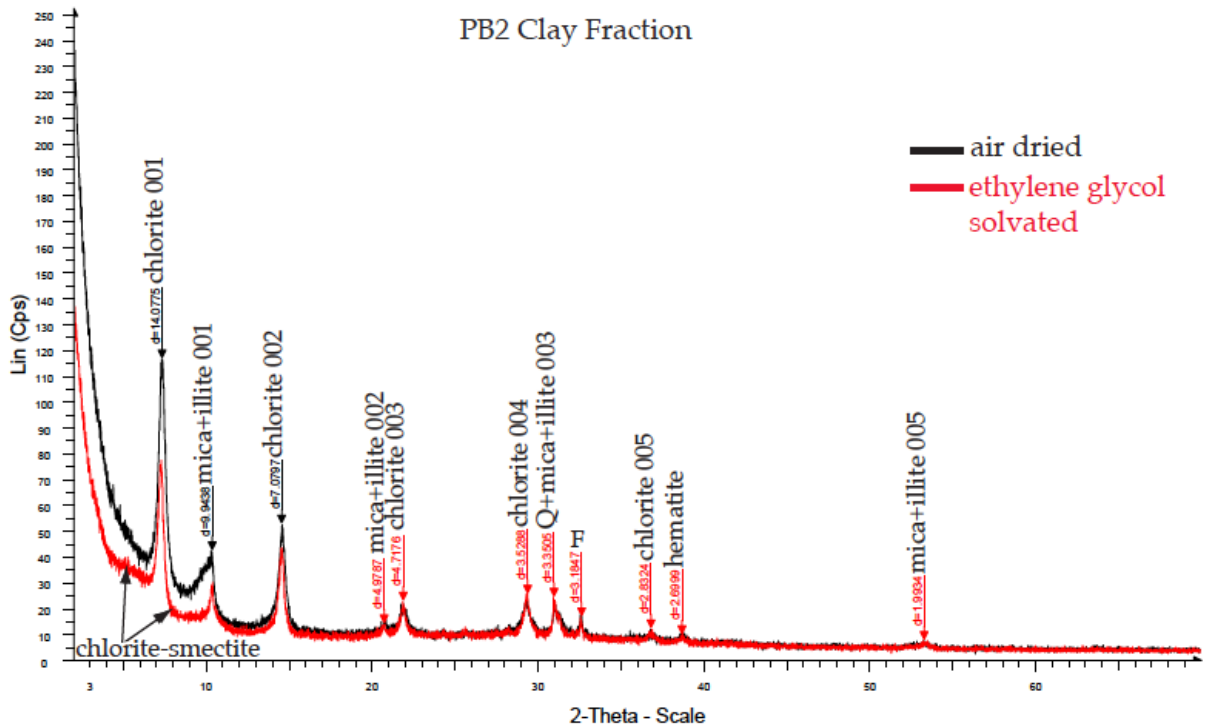
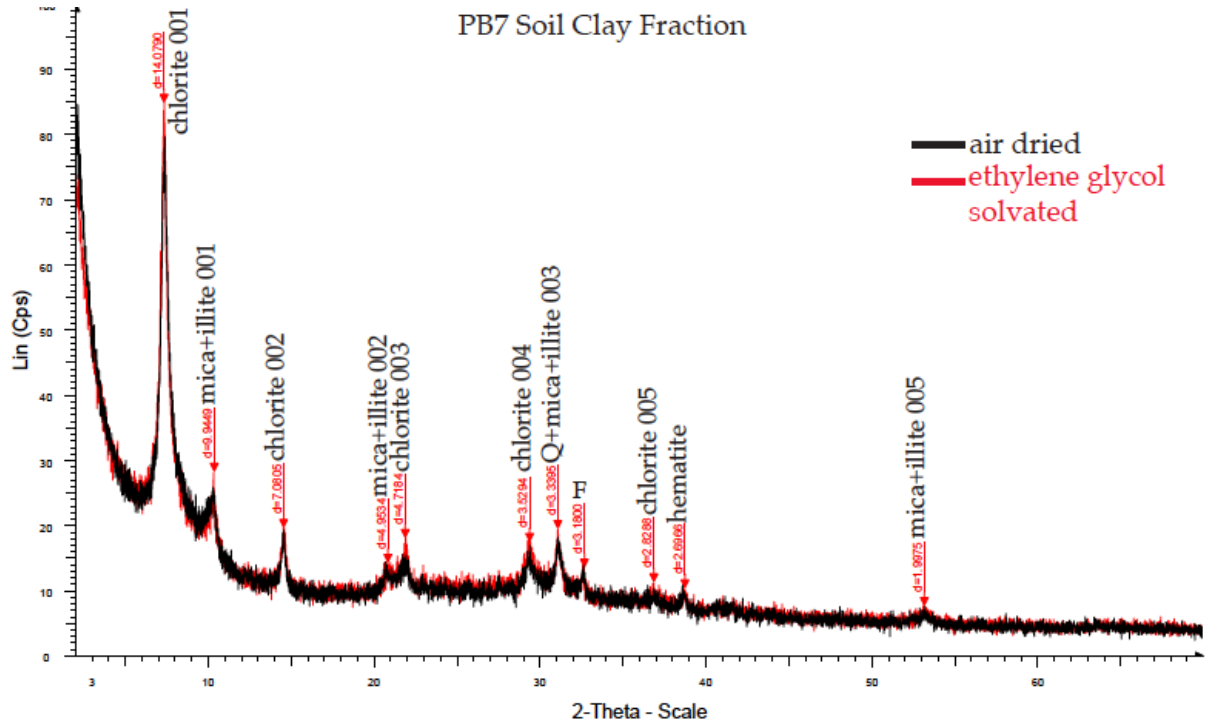


Figure 20. Selected clay fraction diffraction patterns for Portland Formation soil (top) and Portland brownstone (bottom). The patterns were generated using $\text{Co}_{K\alpha}$ radiation.

Table 7a. Portland Formation sample PB7 Soil clay diffraction pattern peak list.

Sample PB7 Soil Air Dried					
Clay	Order of reflection by d-spacing (Å)				
	(001)	(002)	(003)	(004)	(005)
Chlorite	14.07	7.08	4.72	3.53	2.83
Mica/Illite	9.95	4.95	3.33	Absent	1.99
Sample PB7 Soil Ethylene Glycol Saturated					
Clay	Order of reflection by d-spacing (Å)				
	(001)	(002)	(003)	(004)	(005)
Chlorite	14.07	7.08	4.72	3.53	2.83
Mica/Illite	9.95	4.95	3.33	Absent	1.99

Other minerals identified: Quartz (3.34Å), Albite (3.18Å), Hematite (2.69Å)

Table 7b. Portland brownstone sample PB2 clay diffraction pattern peak list.

Sample PB2 Air Dried					
Clay	Order of reflection by d-spacing (Å)				
	(001)	(002)	(003)	(004)	(005)
Chlorite/ Chl-Smectite*	14.07	7.08	4.72	3.53	2.83
Mica/Illite	9.94	4.98	3.35	Absent	1.99
Sample PB2 Ethylene Glycol Saturated					
Clay	Order of reflection by d-spacing (Å)				
	(001)	(002)	(003)	(004)	(005)
Chlorite/ Chl-Smectite*	14.08	7.08	4.72	3.53	2.83
Mica/Illite	9.94	4.98	3.35	Absent	1.99

Other minerals identified: Quartz (3.34Å), Albite (3.18Å), Hematite (2.69Å)

*Chlorite-smectite reflections form as the result of two layer types, chlorite and smectite. The asterisk denotes the pair modulated reflection of mixed layered clays, rather than the usual crystallographic *hkl* notation.

Stanford sandstone

The Stanford sandstone samples contain illite-smectite, kaolinite, goethite, and residual quartz and feldspar in the clay fraction (Fig. 21). Tables 8a and 8b list peaks for selected samples of Stanford sandstone. Samples SU1, SU5, SU7, SU8 show dramatic peak movement after EG-solvation around 11Å and 4Å, and have the appearance of peak between 17-18Å, which indicates presence of smectite. In contrast, samples SU3 and SU4, appear more highly weathered in hand sample and show less movement upon EG solvation. The X-ray patterns for SU3 and SU4 show only slight movement around 10Å with EG-solvation, and no movement around 4Å. Less movement upon EG solvation indicates a higher proportion of illite layers in the mixed illite-smectite. Additionally, the peaks of samples SU3 and SU4 are sharper than the remainder of the samples, indicating the structure of these samples is more ordered than in samples SU1, SU5, SU7, and SU8.

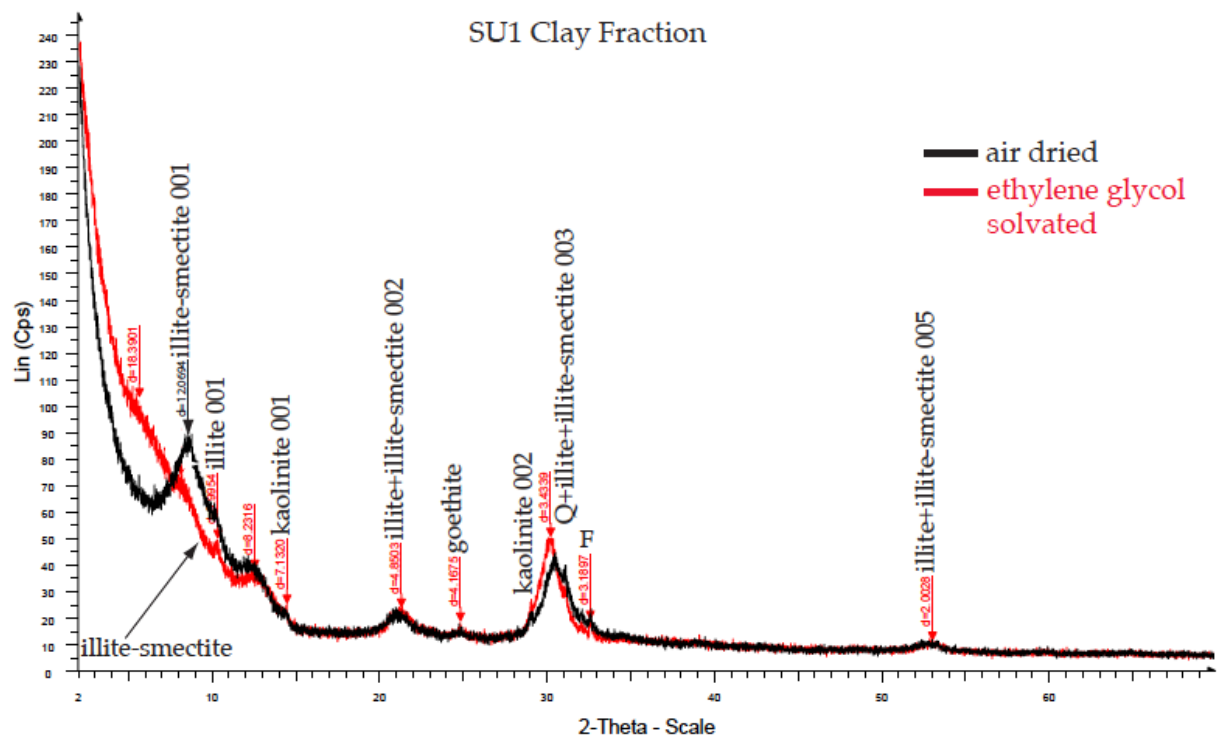
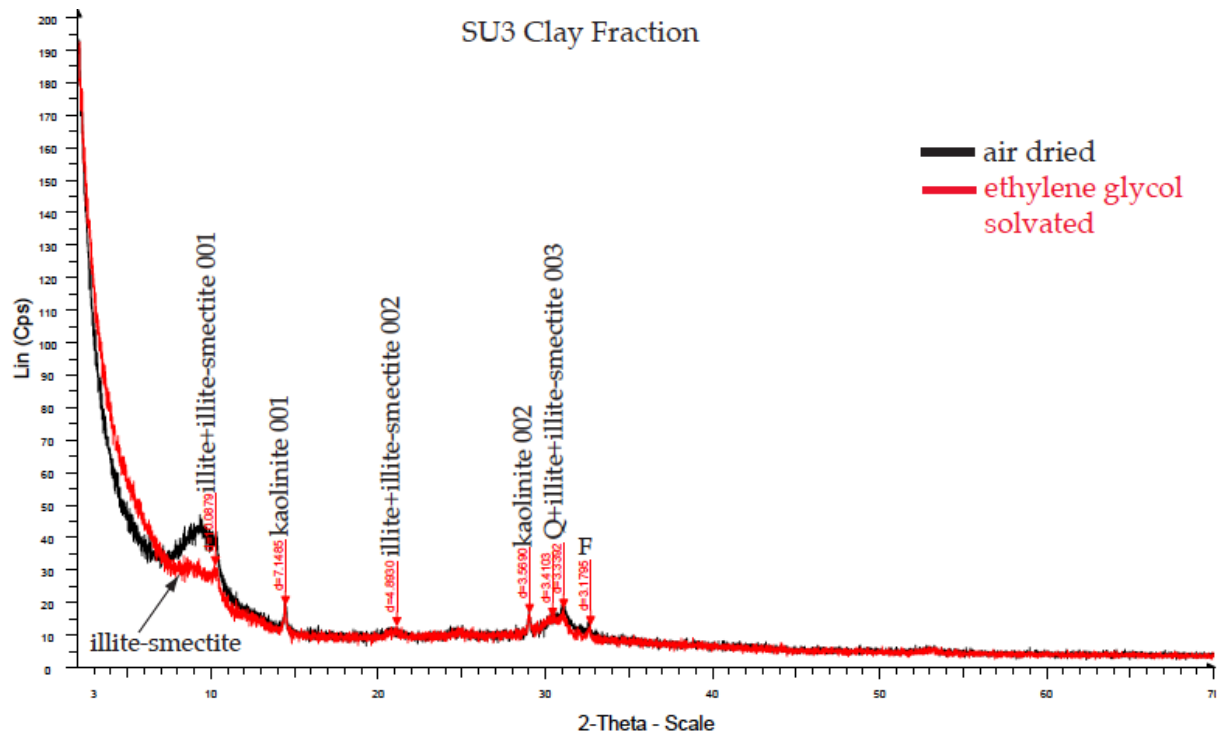


Figure 21. Selected clay fraction diffraction patterns for Stanford sandstone samples SU1 and SU3. The patterns were generated using $\text{CoK}\alpha$ radiation.

Table 8a. Stanford sandstone sample SU3 clay diffraction pattern peak list.

Sample SU3 Air Dried					
Clay	Order of reflection by d-spacing (Å)				
	(001)	(002)	(003)	(004)	(005)
Illite-Smectite*	11.04	4.89	3.41	Absent	Absent
Mica/Illite	11.04	4.89	3.34	Absent	Absent
Kaolinite	7.14	3.57	Absent	Absent	Absent
Sample SU3 Ethylene Glycol Saturated					
Clay	Order of reflection by d-spacing (Å)				
	(001)	(002)	(003)	(004)	(005)
Illite-Smectite*	Unknown	4.89	3.41	Absent	Absent
Micas/Illite	10.08	4.98	3.34	Absent	Absent
Kaolinite	7.14	3.57	Absent	Absent	Absent

Other minerals identified: Quartz (3.34Å), Albite (3.18Å), Goethite (4.18Å)

*Illite-smectite reflections form as the result of two layer types, illite and smectite. The asterisk denotes the pair modulated reflection of mixed layered clays, rather than the usual crystallographic *hkl* notation.

Table 8b. Stanford sandstone sample SU1 clay diffraction pattern peak list.

Sample SU1 Air Dried					
Clay	Order of reflection by d-spacing (Å)				
	(001)	(002)	(003)	(004)	(005)
Illite-Smectite*	12.07	4.85	3.41	Absent	2.00
Mica/Illite	12.07	4.85	3.34	Absent	2.00
Kaolinite	7.13	3.57	Absent	Absent	Absent
Sample SU1 Ethylene Glycol Saturated					
Clay	Order of reflection by d-spacing (Å)				
	(001)	(002)	(003)	(004)	(005)
Illite-Smectite*	18.39	4.85	3.43	Absent	2.00
Micas/Illite	10.08	4.85	3.34	Absent	2.00
Kaolinite	7.13	3.57	Absent	Absent	Absent

Other minerals identified: Quartz (3.34Å), Albite (3.18Å), Goethite (4.17Å)

*See Table 8a for note on illite-smectite.

Comparison of Fresh to Weathered Samples

The most obvious point of comparison in examining fresher to more weathered sandstones was the composition of the clay fraction (Table 9; Figs. 19, 20, and 21). Comparison of fresh and weathered sandstone was constrained by the availability of sample material and the presence of a weathered rind on the samples. Fresher material was located during the course of clay analysis. Mineral weathering in sandstone appears to initially produce more expandable clay components, before reaching a composition with fewer expandable layers.

In the Angkor sandstone, the samples containing smectite and a higher proportion of calcite in the matrix have the potential to weather, particularly if exposed to wetting and drying cycles. These samples also appear stratigraphically at the bottom of the quarry profile, compared to the topmost samples with more chlorite, and smaller amounts of mixed chlorite-smectite. This is analogous in the Portland brownstone, where a soil sample confirms that the more weathered soil contains only chlorite in the clay fraction, while the brownstone contains a small proportion of chlorite-smectite. Likewise, Stanford sandstone contains mixed illite-smectite in the clay fraction with a large proportion of swelling smectite layers, while the outer hardened crust contains illite-smectite, with a much higher proportion of illite to smectite.

Table 9. Clay fraction comparison of fresh to weathered samples.

Locality	Clay fraction of fresh material	Clay fraction of weathered material	Comparison
Kulen Mountain	Chlorite-smectite Mica-illite Smectite Calcite	Chlorite-smectite Mica-illite	Fewer expandable clays and no calcite (which is highly soluble) in weathered material
Portland, Connecticut	Chlorite-smectite Mica-illite	Chlorite Mica-illite	No expandable clays in the overlying soil compared to the sandstone
Stanford, California	Smectite Illite-smectite Kaolinite Limonite	Illite-smectite Kaolinite	Small proportion of expandable smectite layers in the illite-smectite in the weathered material.

Electron Microprobe Analysis

Electron microprobe analysis was conducted to look at the phases most abundant in sandstone and examine their susceptibility to weathering. The mineral groups examined in this study were alkali feldspar, plagioclase feldspar, mica, and chlorite. Table 10 summarizes the microprobe results.

Feldspars exist as a solid solution between potassium and sodium to form alkali feldspars, and sodium and calcium to form plagioclase feldspars. The alkali feldspar in these sandstones is potassium rich and thus has a low weathering rate. This analysis primarily focused on the plagioclase solid solution series between the albite (Na-rich end-member) and anorthite (Ca-rich end-member) because calcium-rich plagioclase weathers more quickly at earth surface conditions.

Micas and chlorites were examined for their iron and potassium content. Iron oxidizes, forming hematite acting as a secondary cement for flakes of mica and chlorite. Although

muscovite mica is more resistant to weathering at earth surface conditions than biotite and chlorite, the presence of iron and magnesium in muscovite can induce weathering. Loss of potassium from biotite and muscovite is also an indicator of alteration.

Table 10. Summary of microprobe results.

Sandstone Type	Potassium Feldspar	Plagioclase Feldspar	Biotite Mg/Mg+Fe	Chlorite Mg/Mg+Fe	Muscovite Fe in atoms per formula unit	Muscovite Mg in atoms per formula unit
Angkor sandstone	Ab ₂₋₁₅ An ₀ Or ₈₇₋₉₈	Ab ₈₀₋₉₉ An ₁₋₁₈ Or ₀₋₂	0.41-0.51	0.45-0.52	0.05-0.32	0.02-0.17
Portland brownstone	Ab ₄₋₇ An ₀ Or ₉₂₋₉₅	Ab ₈₀₋₉₅ An ₅₋₁₈ Or ₀₋₁	0.49-0.54	0.38-0.65	0.04-0.18	0.04-0.18
Stanford sandstone	Ab ₆₋₁₁ An ₀ Or ₈₈₋₉₃	Ab ₇₁₋₈₇ An ₁₂₋₂₆ Or ₀₋₄	0.39-0.57	n/a	0.04	0.05

Kulen Mountain sandstone

Clastic Grains

Both potassium and plagioclase feldspars were analyzed in the Kulen Mountain feldspathic arenites (Tables 11 and 12). According to the modal analysis, feldspars make up 27-37% of framework grains in these samples (Table 5)(Carò and IM, 2012). Microprobe analyses show potassium feldspar of composition (Ab₂₋₁₅, An₀, Or₈₇₋₉₈). It also reveals a bimodal mixture of albite (Ab₉₃₋₉₉, An₁₋₅, Or₀₋₁) and oligoclase (Ab₈₀₋₈₉, An₈₋₁₈, Or₀₋₂). Zoned feldspar was not found in these samples.

Muscovite, biotite, and chlorite all occur in the Kulen Mountain sandstone samples used in this study (Tables 13, 14, and 15). Seven analyses of muscovite contain detectable levels of magnesium and iron. Potassium contents in muscovite were routinely less (0.72-0.92 atoms per formula unit) than the stoichiometric 1 K apfu.

Table 11. Potassium feldspar microprobe analyses for Kulen Mountain sandstone.

	104B					109B				
	2	3	4	6		1	2	3	4	5
SiO₂	64.57	64.54	64.25	64.78	SiO₂	64.56	64.26	64.54	63.93	65.02
TiO₂	0.05	bdl	0.04	bdl	TiO₂	0.08	bdl	bdl	bdl	bdl
FeO	0.12	bdl	0.10	bdl	FeO	bdl	0.13	bdl	bdl	0.13
Al₂O₃	17.72	17.65	18.38	17.75	Al₂O₃	18.38	18.11	18.63	18.02	18.32
MgO	bdl	bdl	bdl	bdl	MgO	0.00	bdl	bdl	bdl	0.04
CaO	bdl	bdl	0.05	bdl	CaO	0.09	0.16	0.06	0.14	bdl
MnO	bdl	bdl	bdl	bdl	MnO	bdl	0.00	bdl	0.11	0.30
K₂O	16.06	16.30	16.46	15.15	K₂O	14.77	16.10	15.37	15.29	16.44
Na₂O	0.61	0.53	0.43	1.19	Na₂O	1.43	0.25	0.83	1.65	0.56
BaO	bdl	bdl	0.14	0.16	BaO	0.38	0.38	0.25	0.15	bdl
Total	99.11	99.02	99.85	99.03	Total	99.69	99.39	99.67	99.29	100.82
Numbers of ions based on 8 O										
Si	3.01	3.02	2.99	3.02	Si	2.99	3.00	2.99	2.98	2.99
Ti	0.00	0.00	0.00	0.00	Ti	0.00	0.00	0.00	0.00	0.00
Fe	0.00	0.00	0.00	0.00	Fe	0.00	0.01	0.00	0.00	0.01
Al	0.97	0.97	1.01	0.97	Al	1.00	1.00	1.02	0.99	0.99
Mg	0.00	0.00	0.00	0.00	Mg	0.00	0.00	0.00	0.00	0.00
Ca	0.00	0.00	0.00	0.00	Ca	0.00	0.01	0.00	0.01	0.00
Mn	0.00	0.00	0.00	0.00	Mn	0.00	0.00	0.00	0.00	0.01
K	0.96	0.97	0.98	0.90	K	0.87	0.96	0.91	0.91	0.96
Na	0.06	0.05	0.04	0.11	Na	0.13	0.02	0.07	0.15	0.05
Ba	0.00	0.00	0.00	0.00	Ba	0.01	0.01	0.00	0.00	0.00
Mol per cent end-members										
Ab	5.5	4.7	3.8	10.7	Ab	12.8	2.3	7.5	14.0	4.9
An	0.0	0.0	0.2	0.0	An	0.4	0.8	0.3	0.6	0.0
Or	94.6	95.3	96.0	89.4	Or	86.8	96.9	92.2	85.4	95.1

bdl= below detection limit

Table 12. Plagioclase feldspar microprobe analyses for Kulen Mountain sandstone.

104B							109B				
	1	2	3	4	5	6	1	2	4	5	
SiO₂	66.89	64.25	66.83	68.04	63.43	64.18	SiO₂	65.63	67.51	63.70	66.51
TiO₂	bdl	bdl	bdl	bdl	0.05	0.05	TiO₂	bdl	bdl	bdl	bdl
FeO	0.18	bdl	bdl	bdl	0.05	bdl	FeO	bdl	bdl	0.18	0.15
Al₂O₃	20.06	21.62	19.88	19.19	22.67	22.01	Al₂O₃	20.60	19.27	22.50	19.92
MgO	bdl	bdl	0.05	bdl	bdl	0.00	MgO	bdl	bdl	0.04	bdl
CaO	0.99	3.02	0.35	0.26	3.73	3.45	CaO	1.69	0.85	3.75	1.24
MnO	bdl	bdl	bdl	bdl	bdl	0.11	MnO	bdl	bdl	bdl	bdl
K₂O	0.21	0.22	0.15	0.00	0.16	0.14	K₂O	0.48	0.14	0.11	0.08
Na₂O	11.19	9.71	11.38	11.20	9.05	9.61	Na₂O	10.29	10.70	9.55	10.92
BaO	bdl	bdl	bdl	bdl	bdl	bdl	BaO	bdl	bdl	0.17	bdl
Total	99.52	98.82	98.63	98.70	99.14	99.54	Total	98.76	98.48	100.00	98.83
Numbers of ions based on 8 O											
Si	2.95	2.86	2.96	3.00	2.82	2.84	Si	2.92	2.99	2.82	2.95
Ti	0.00	0.00	0.00	0.00	0.00	0.00	Ti	0.00	0.00	0.00	0.00
Fe	0.01	0.00	0.00	0.00	0.00	0.00	Fe	0.00	0.00	0.01	0.01
Al	1.04	1.14	1.04	1.00	1.19	1.15	Al	1.08	1.01	1.17	1.04
Mg	0.00	0.00	0.00	0.00	0.00	0.00	Mg	0.00	0.00	0.00	0.00
Ca	0.05	0.14	0.02	0.01	0.18	0.16	Ca	0.08	0.04	0.18	0.06
Mn	0.00	0.00	0.00	0.00	0.00	0.00	Mn	0.00	0.00	0.00	0.00
K	0.01	0.01	0.01	0.00	0.01	0.01	K	0.03	0.01	0.01	0.00
Na	0.96	0.84	0.98	0.96	0.78	0.83	Na	0.89	0.92	0.82	0.94
Ba	0.00	0.00	0.00	0.00	0.00	0.00	Ba	0.00	0.00	0.00	0.00
Mol per cent end-members											
Ab	94.2	84.2	97.5	98.7	80.7	82.8	Ab	89.2	95.0	81.7	93.7
An	4.6	14.5	1.6	1.3	18.4	16.4	An	8.1	4.2	17.7	5.9
Or	1.2	1.3	0.9	0.0	1.0	0.8	Or	2.7	0.8	0.6	0.5

bdl=below detection limit

Table 13. Muscovite microprobe analyses for Kulen Mountain sandstone.

	104B					109B					
	1	2	3	4		1	1a	2	2a	2b	3
SiO₂	46.51	45.09	46.14	45.76	SiO₂	45.01	45.27	45.29	45.97	46.97	44.64
TiO₂	0.48	bdl	0.69	1.36	TiO₂	0.13	0.38	0.44	0.46	0.33	0.57
FeO	2.06	0.99	3.24	1.13	FeO	1.29	1.21	1.55	1.72	1.81	5.85
Al₂O₃	33.59	35.06	30.78	33.57	Al₂O₃	34.27	33.94	32.62	32.63	31.76	28.24
MgO	1.34	0.72	0.74	0.99	MgO	0.19	0.73	1.34	1.32	1.38	1.81
CaO	bdl	bdl	bdl	bdl	CaO	0.13	0.03	0.07	0.12	0.05	0.06
MnO	bdl	bdl	bdl	bdl	MnO	0.21	bdl	bdl	bdl	bdl	bdl
K₂O	11.05	10.77	8.92	10.14	K₂O	10.07	10.27	10.56	10.34	10.45	11.21
Na₂O	0.31	0.74	0.13	0.70	Na₂O	0.60	0.79	0.30	0.30	0.27	0.18
BaO	0.28	bdl	0.10	0.24	BaO	0.21	0.29	0.12	0.19	bdl	0.41
Total	95.62	93.37	90.75	93.89	Total	92.12	92.90	92.29	93.05	93.02	92.98
Numbers of ions based on 10 O											
Si	2.83	2.79	2.93	2.81	Si	2.82	2.82	2.84	2.86	2.92	2.88
Ti	0.02	0.00	0.03	0.06	Ti	0.01	0.02	0.02	0.02	0.02	0.03
Fe	0.10	0.05	0.17	0.06	Fe	0.07	0.06	0.08	0.09	0.09	0.32
Al	2.41	2.56	2.30	2.43	Al	2.53	2.49	2.41	2.39	2.32	2.14
Mg	0.12	0.07	0.07	0.09	Mg	0.02	0.07	0.13	0.12	0.13	0.17
Ca	0.00	0.00	0.00	0.00	Ca	0.01	0.00	0.00	0.01	0.00	0.00
Mn	0.00	0.00	0.00	0.00	Mn	0.01	0.00	0.00	0.00	0.00	0.00
K	0.86	0.85	0.72	0.80	K	0.81	0.82	0.85	0.82	0.83	0.92
Na	0.04	0.09	0.02	0.08	Na	0.07	0.09	0.04	0.04	0.03	0.02
Ba	0.01	0.00	0.00	0.01	Ba	0.01	0.01	0.00	0.00	0.00	0.01

bdl=below detection limit

Table 14. Biotite microprobe analyses for Kulen Mountain sandstone.

104B			
	1	2	3
SiO₂	33.84	29.88	34.57
Al₂O₃	18.29	17.62	17.13
MgO	10.58	9.94	11.58
FeO	19.16	25.67	20.57
MnO	0.20	0.65	0.61
CaO	0.08	0.28	0.34
K₂O	7.08	2.46	2.64
Na₂O	0.07	0.03	0.07
TiO₂	2.69	2.39	1.03
Cr₂O₃	bdl	0.05	0.05
Total	91.99	88.97	88.58
Number of ions based on 10 O			
Si	2.41	2.24	2.50
Al	1.53	1.56	1.46
Mg	1.12	1.11	1.25
Fe	1.14	1.61	1.25
Mn	0.01	0.04	0.04
Ca	0.01	0.02	0.03
K	0.64	0.24	0.24
Na	0.01	0.00	0.01
Ti	0.14	0.13	0.06
Cr	0.00	0.00	0.00
Mg number $Mg/(Mg + Fe) \times 100$			
	49.6	40.8	50.1

bdl=below detection limit

Table 15. Chlorite microprobe analyses for Kulen Mountain sandstone.

	104B	109B
	1	1
SiO₂	29.62	29.73
Al₂O₃	15.60	15.28
MgO	11.65	13.70
FeO	25.20	22.37
MnO	0.56	0.53
CaO	0.45	0.18
K₂O	0.73	0.26
Na₂O	0.10	0.05
TiO₂	1.93	1.43
Cr₂O₃	bdl	
Total	85.84	83.69
Number of ions on the basis of 28 O		
Si	6.40	6.47
Al	3.97	3.92
Mg	3.75	4.44
Fe	4.55	4.07
Mn	0.10	0.10
Ca	0.10	0.04
K	0.20	0.07
Na	0.04	0.02
Ti	0.31	0.23
Cr	0.00	0.00
Mg number $Mg/(Mg + Fe) \times 100$		
	45.2	52.2

bdl=below detection limit

Three biotite analyses were done on the Kulen Mountain sandstone. The presence of very fine-grained iron oxide inclusions in the biotite made targeting of “unaltered” biotite difficult. All of the biotite analyses contain comparable amounts of iron and magnesium. Potassium contents in the biotite were low, routinely less (0.24 to 0.64 apfu) than the stoichiometric 1K apfu.

Chlorite grains contain abundant, fine-grained inclusions of iron oxide that made location of suitable “spots” for microprobe analysis difficult. The chlorite analyses have comparable amounts of iron and magnesium.

Accessory Minerals

Reconnaissance of samples through EDS allowed for the identification of the accessory minerals garnet, zircon, epidote, muscovite, biotite, chlorite, apatite, zeolite, sphene, rutile, and ilmenite in the Kulen Mountain sandstone (Fig. 22). Element mapping allowed for the more specific identification of allanite, the cerium rich variety of epidote. Figure 22 shows cerium mapped on an allanite grain. With the exception of the micas and chlorites, none of these accessory minerals are expected to weather rapidly in the time scale of the one thousand year exposure in the quarry (Pettijohn, 1941; Taylor and Eggleton, 2001).

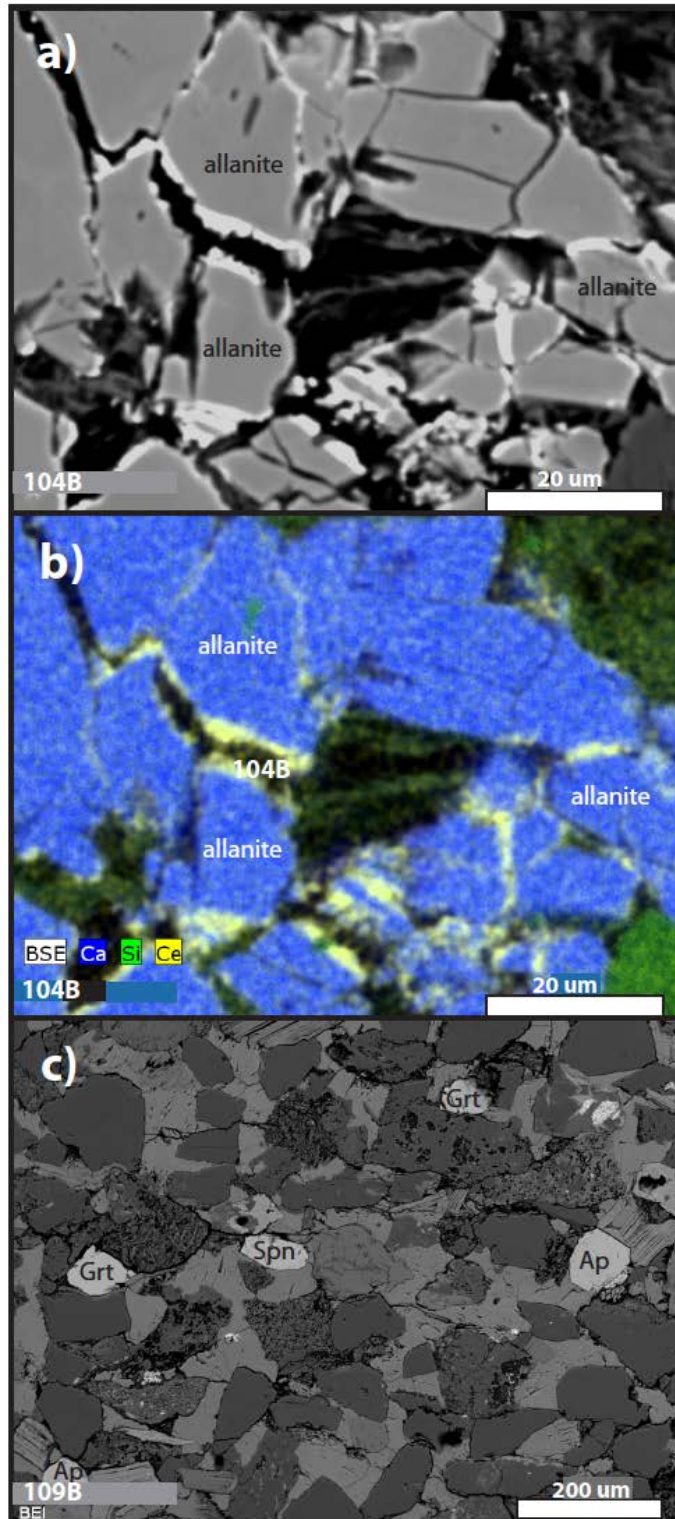


Figure 22. Identification of accessory minerals in Kulen Mountain sandstone. (a) Backscatter image and (b) element map of the Ce-bearing epidote mineral allanite, (c) backscatter image showing garnet, apatite, and sphene. For mineral abbreviations see Tables 2, 3, and 4.

Cement and Matrix

Both the chlorite-rich sandstone and the calcite-rich sandstone identified in XRD analysis (Fig. 19) contain abundant cement (Fig. 23). Chlorite, quartz, and feldspar cement is present in Sample 104B, while calcite cement, with lesser amounts of quartz and feldspar cement, predominates in Sample 109B. The chlorite-rich sandstone samples have almost no calcite present in the matrix, while the calcite cemented samples have a large amount of calcite in the matrix (Fig. 24). There is both detrital chlorite and chlorite cement in the Kulen Mountain sandstone. Detrital chlorite, like the heavily weathered biotite grains, often contains hematite cement and oxide inclusions.

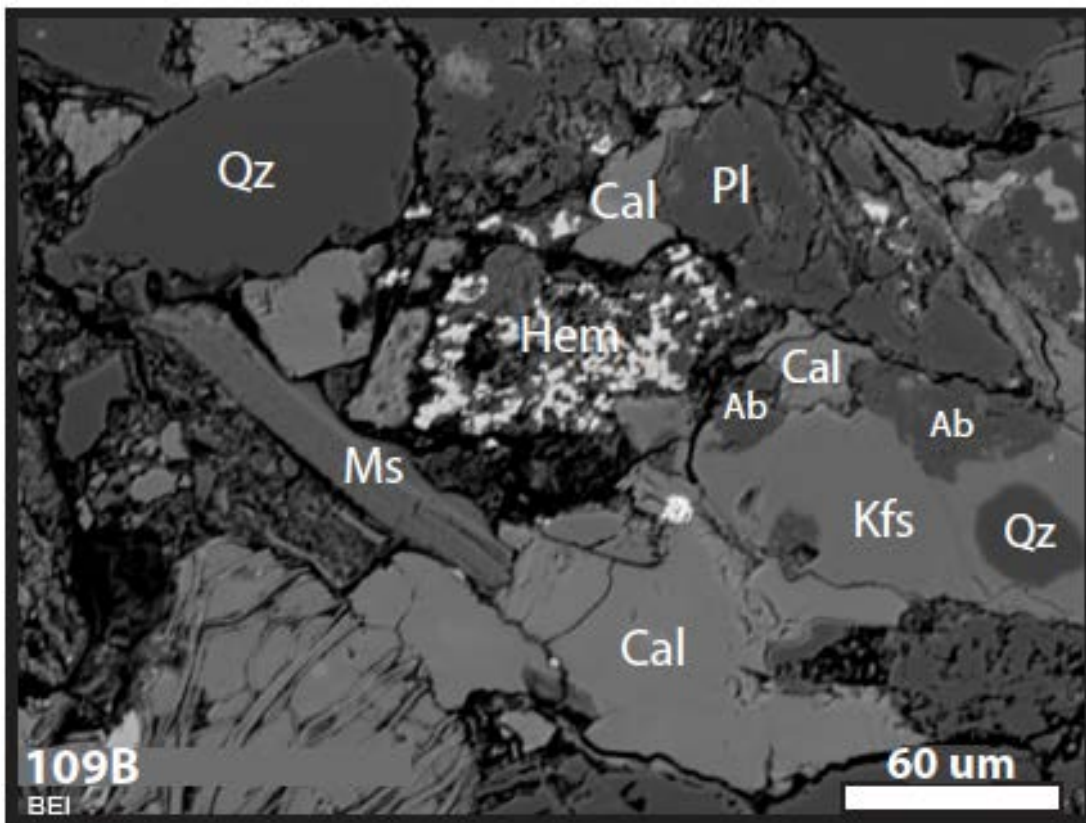


Figure 23. Identification of cement in Kulen Mountain sandstone. Calcite cement of plagioclase (Pl) grain and potassium feldspar (Kfs), and albite cementing potassium feldspar. For additional abbreviations see Tables 2, 3, and 4.

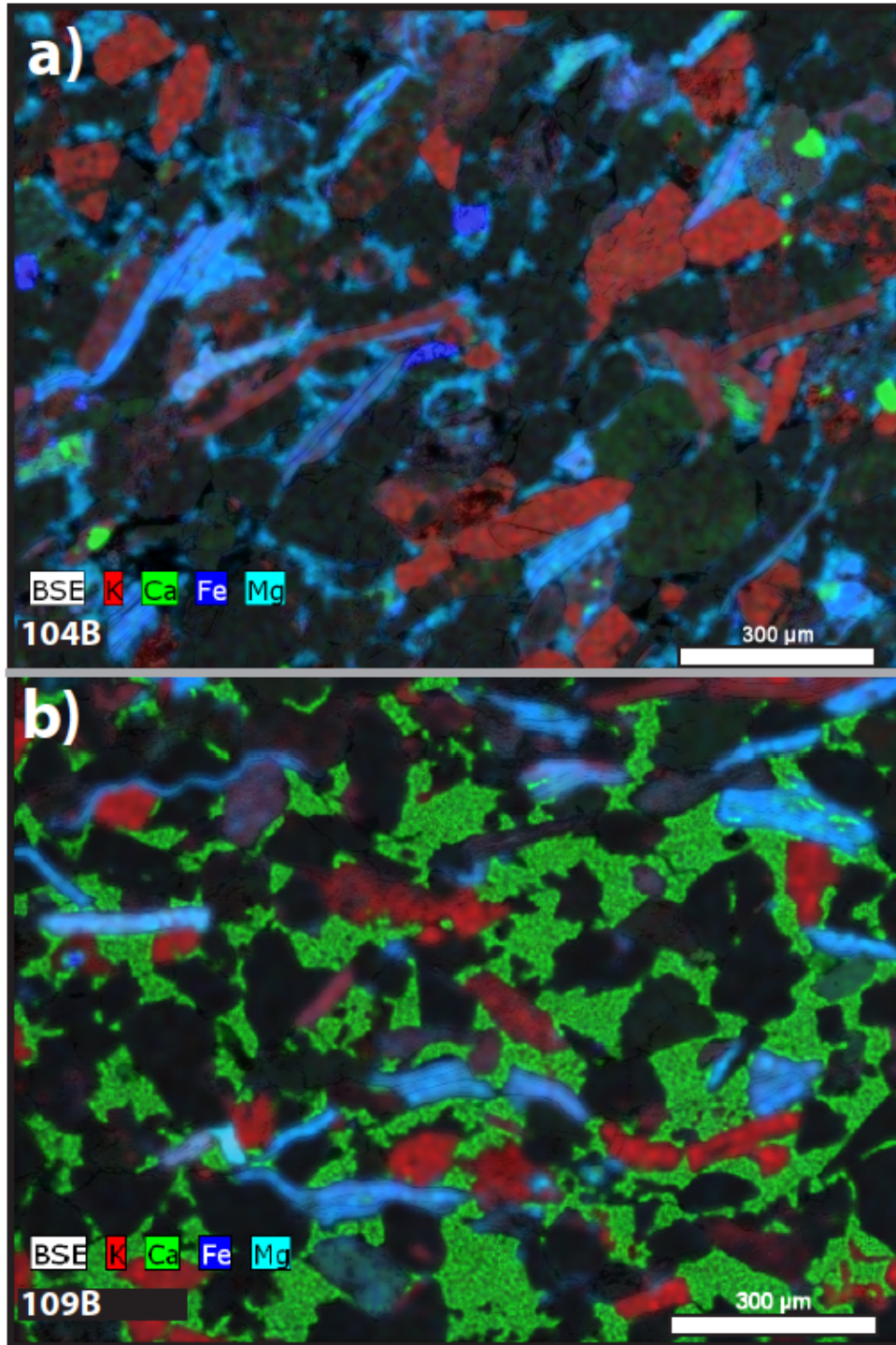


Figure 24. Comparison of the matrix in Kulen Mountain sandstone. (a) Element map of sample 104B showing no calcite in the matrix, (b) Element map of sample 109B showing abundant calcite in the matrix of the sandstone. Green indicates calcium in the calcite cement. Iron is mapped in blue. The elongate blue grains represent chlorite. Blue in the matrix is iron oxide cement.

Portland brownstone

Clastic Grains

Potassium and plagioclase feldspars were analyzed in the Portland feldspathic arenite (Tables 16, 17a, and 17b). Feldspars comprise 50-51% of framework grains in these samples (Table 5). Microprobe analyses show potassium feldspar of composition (Ab₄₋₇, An₀, Or₉₂₋₉₅). It also reveals a bimodal mixture of albite (Ab₉₁₋₉₅, An₅₋₈, Or₀₋₁) and oligoclase (Ab₈₀₋₈₆, An₁₃₋₁₈, Or₀₋₁). No zoning was found in the feldspar.

Table 16. Potassium feldspar microprobe analyses for Portland brownstone.

	PB2	PB6	PB7	PB8
	1	3	1	1
SiO₂	64.49	64.33	63.91	64.37
Al₂O₃	18.55	18.81	18.52	18.36
MgO	bdl	bdl	bdl	bdl
FeO	bdl	bdl	bdl	bdl
MnO	bdl	bdl	bdl	bdl
CaO	bdl	bdl	bdl	bdl
K₂O	16.54	16.55	16.19	15.92
Na₂O	0.56	0.62	0.78	0.81
TiO₂	bdl	bdl	bdl	bdl
Total	100.14	100.31	99.39	99.46
Numbers of ions based on 8 O				
Si	2.98	2.97	2.98	2.99
Al	1.01	1.02	1.02	1.01
Mg	0.00	0.00	0.00	0.00
Fe	0.00	0.00	0.00	0.00
Mn	0.00	0.00	0.00	0.00
Ca	0.00	0.00	0.00	0.00
K	0.98	0.98	0.96	0.94
Na	0.05	0.06	0.07	0.07
Ti	0.00	0.00	0.00	0.00
Mol per cent end-members				
Ab	4.9	5.4	6.8	7.1
An	0.0	0.0	0.0	0.0
Or	95.1	94.6	93.2	92.9

bdl=below detection limit

Table 17a. Plagioclase feldspar microprobe analyses for Portland brownstone.

	PB2					PB6		
	1	2	3	4	5	2	5	6
SiO₂	64.54	66.85	64.86	67.47	65.14	66.09	63.80	65.06
Al₂O₃	22.03	20.76	22.12	20.50	22.29	20.94	22.33	21.90
MgO	bdl	bdl	bdl	bdl	bdl	bdl	bdl	bdl
FeO	bdl	bdl	bdl	0.11	bdl	0.07	bdl	bdl
MnO	bdl	bdl	bdl	bdl	bdl	bdl	bdl	bdl
CaO	2.85	1.21	3.27	0.97	3.50	1.61	3.43	2.83
K₂O	0.10	0.11	0.21	0.08	0.04	0.13	0.04	0.06
Na₂O	10.39	11.08	9.90	11.37	9.71	10.26	9.36	9.84
TiO₂	bdl	bdl	bdl	bdl	bdl	bdl	bdl	0.06
Total	99.92	100.02	100.35	100.51	100.68	99.11	98.96	99.76
Numbers of ions based on 8 O								
Si	2.85	2.93	2.85	2.94	2.85	2.92	2.84	2.87
Al	1.15	1.07	1.15	1.05	1.15	1.09	1.17	1.14
Mg	0.00	0.00	0.00	0.00	0.00	0.00	0.00	0.00
Fe	0.00	0.00	0.00	0.00	0.00	0.00	0.00	0.00
Mn	0.00	0.00	0.00	0.00	0.00	0.00	0.00	0.00
Ca	0.13	0.06	0.15	0.05	0.16	0.08	0.16	0.13
K	0.01	0.01	0.01	0.00	0.00	0.01	0.00	0.00
Na	0.89	0.94	0.84	0.96	0.82	0.88	0.81	0.84
Ti	0.00	0.00	0.00	0.00	0.00	0.00	0.00	0.00
Mol per cent end-members								
Ab	86.4	93.7	83.6	95.0	83.2	91.3	83.0	86.0
An	13.1	5.6	15.2	4.5	16.6	7.9	16.8	13.7
Or	0.6	0.6	1.2	0.5	0.2	0.8	0.2	0.4

bdl=below detection limit

Table 17b. Plagioclase feldspar microprobe analyses for Portland brownstone.

	PB7			PB8				
	1	3	9	1	3	4	5	6
SiO₂	63.97	64.39	64.76	64.67	64.75	63.69	64.79	64.67
Al₂O₃	22.45	21.89	22.05	21.53	22.00	22.62	21.63	21.61
MgO	bdl	bdl	bdl	bdl	bdl	bdl	bdl	bdl
FeO	bdl	bdl	0.08	bdl	bdl	bdl	bdl	bdl
MnO	bdl	bdl	bdl	bdl	bdl	bdl	bdl	bdl
CaO	3.36	2.92	2.82	2.77	3.04	3.80	2.90	2.82
K₂O	0.20	0.18	0.23	0.05	0.23	0.18	0.08	0.15
Na₂O	9.36	9.78	9.73	10.05	9.58	9.41	9.62	10.13
TiO₂	0.05	bdl	bdl	bdl	bdl	bdl	0.04	bdl
Total	99.39	99.17	99.67	99.07	99.60	99.69	99.06	99.38
Numbers of ions based on 8 O								
Si	2.84	2.86	2.86	2.87	2.86	2.82	2.87	2.87
Al	1.17	1.15	1.15	1.13	1.15	1.18	1.13	1.13
Mg	0.00	0.00	0.00	0.00	0.00	0.00	0.00	0.00
Fe	0.00	0.00	0.00	0.00	0.00	0.00	0.00	0.00
Mn	0.00	0.00	0.00	0.00	0.00	0.00	0.00	0.00
Ca	0.16	0.14	0.13	0.13	0.14	0.18	0.14	0.13
K	0.01	0.01	0.01	0.00	0.01	0.01	0.00	0.01
Na	0.80	0.84	0.83	0.87	0.82	0.81	0.83	0.87
Ti	0.00	0.00	0.00	0.00	0.00	0.00	0.00	0.00
Mol per cent end-members								
Ab	82.5	85.0	85.0	86.5	84.0	80.9	85.3	86.0
An	16.3	14.0	13.6	13.2	14.7	18.1	14.2	13.2
Or	1.2	1.0	1.3	0.3	1.3	1.0	0.5	0.8

bdl=below detection limit

Muscovite, biotite, and chlorite all occur in the Portland brownstone samples used in this study (Tables 18, 19, and 20). All twelve analyses of muscovite contain detectable levels of magnesium and iron. Potassium contents in muscovite were routinely less (0.69-0.86 apfu) than the stoichiometric 1 K apfu.

Twelve biotite analyses were done on the Portland brownstone. The presence of very fine-grained iron oxide inclusions in the biotite made targeting of “unaltered” biotite difficult. Biotite analyses contain variable amounts of iron and magnesium. Magnesium numbers ($Mg/Mg+Fe \times 100$) range from 47.2-58.5. Potassium contents in the biotite were low, routinely less (0.32 to 0.78 apfu) than the stoichiometric 1K apfu.

Chlorite grains contain abundant, fine-grained inclusions of iron oxide that made location of suitable “spots” for microprobe analysis difficult. The chlorite analyses have variable amounts of iron and magnesium. Magnesium numbers ($Mg/Mg+Fe \times 100$) range from 38.5-65.9.

Accessory Minerals

The reconnaissance of accessory minerals through EDS showed ilmenite, rutile, apatite, magnetite, amphibole, zircon, and garnet to be present in the Portland brownstone (Figure 25). Garnet was an abundant component in the accessory mineral assemblage. Aside from the micas and chlorites, the remainder of the accessory mineral phases is not susceptible to weathering on the time scale of two hundred years where Portland brownstone has popularly been used as a building material (Pettijohn, 1941; Taylor and Eggleton, 2001).

Table 18. Muscovite microprobe analyses for Portland brownstone.

	PB2			PB6				PB7		PB8			
	1	2	3	1	2	3		1	2	1	2	3	4
SiO₂	44.95	44.32	45.83	45.15	44.03	45.35	SiO₂	45.43	45.55	44.70	44.53	44.90	43.92
Al₂O₃	33.99	34.41	36.65	35.66	35.40	35.06	Al₂O₃	31.15	34.33	36.22	34.25	33.62	32.82
MgO	1.30	0.88	0.50	0.58	0.74	0.68	MgO	1.89	0.98	0.40	0.72	0.78	0.89
FeO	1.54	0.71	1.03	1.28	1.57	1.63	FeO	3.35	1.92	0.86	2.65	1.34	0.85
MnO	bdl	bdl	bdl	bdl	bdl	bdl	MnO	bdl	bdl	bdl	0.09	bdl	bdl
CaO	0.04	bdl	bdl	bdl	0.03	bdl	CaO	bdl	bdl	0.07	bdl	0.11	bdl
K₂O	10.33	8.87	9.02	9.27	9.73	10.85	K₂O	10.70	10.86	9.96	9.11	9.78	9.57
Na₂O	0.43	0.77	1.33	0.99	0.59	0.52	Na₂O	0.27	0.29	0.60	1.21	0.66	1.02
TiO₂	0.20	1.17	0.53	0.92	0.98	0.22	TiO₂	0.34	1.13	0.13	0.17	1.06	0.96
Total	92.78	91.12	94.89	93.84	93.06	94.31	Total	93.11	95.06	92.94	92.72	92.25	90.03
Numbers of ions based on 10 O													
Si	2.80	2.78	2.76	2.76	2.73	2.79	Si	2.85	2.78	2.76	2.78	2.80	2.81
Al	2.50	2.54	2.60	2.57	2.59	2.54	Al	2.31	2.47	2.64	2.52	2.48	2.47
Mg	0.12	0.08	0.04	0.05	0.07	0.06	Mg	0.18	0.09	0.04	0.07	0.07	0.08
Fe	0.08	0.04	0.05	0.07	0.08	0.08	Fe	0.18	0.10	0.04	0.14	0.07	0.05
Mn	0.00	0.00	0.00	0.00	0.00	0.00	Mn	0.00	0.00	0.00	0.00	0.00	0.00
Ca	0.00	0.00	0.00	0.00	0.00	0.00	Ca	0.00	0.00	0.00	0.00	0.01	0.00
K	0.82	0.71	0.69	0.72	0.77	0.85	K	0.86	0.85	0.78	0.73	0.78	0.78
Na	0.05	0.09	0.16	0.12	0.07	0.06	Na	0.03	0.03	0.07	0.15	0.08	0.13
Ti	0.01	0.06	0.02	0.04	0.05	0.01	Ti	0.02	0.05	0.01	0.01	0.05	0.05

bdl=below detection limit

Table 19. Biotite microprobe analyses for Portland brownstone.

	PB2				PB6		PB7			PB8			
	1	3	4	5	1	2	1	2	3	1	2	3	
SiO₂	35.31	33.33	32.24	35.72	36.94	36.61	SiO₂	34.56	30.56	36.61	32.17	37.75	37.89
Al₂O₃	19.03	19.15	18.16	18.58	18.36	17.57	Al₂O₃	18.02	16.95	18.14	19.78	17.01	16.88
MgO	9.85	8.55	10.45	10.47	10.48	10.45	MgO	10.43	12.50	10.08	11.16	11.01	11.07
FeO	17.35	21.19	20.83	16.81	15.58	16.66	FeO	17.24	21.65	15.12	20.44	14.62	14.01
MnO	0.29	0.14	0.16	0.19	0.10	0.23	MnO	0.08	0.46	0.12	0.38	0.13	0.21
CaO	0.05	0.07	0.21	0.11	0.10	0.10	CaO	0.31	0.02	0.17	bdl	0.09	0.11
K₂O	8.41	7.60	5.10	6.76	7.74	7.19	K₂O	6.52	3.34	7.21	5.58	8.67	7.49
Na₂O	0.17	0.23	0.17	0.34	0.06	0.05	Na₂O	0.19	bdl	0.26	0.27	0.17	0.19
TiO₂	2.71	2.79	1.32	1.54	1.59	1.57	TiO₂	1.47	2.76	1.63	2.11	1.52	1.70
Total	93.17	93.05	88.65	90.50	90.96	90.44	Total	88.83	88.24	89.34	91.90	90.97	89.57
Number of ions based on 10 O													
Si	2.46	2.37	2.38	2.53	2.59	2.59	Si	2.51	2.27	2.60	2.29	2.65	2.67
Al	1.56	1.61	1.58	1.55	1.52	1.47	Al	1.54	1.49	1.52	1.66	1.41	1.40
Mg	1.02	0.91	1.15	1.11	1.10	1.10	Mg	1.13	1.39	1.07	1.19	1.15	1.17
Fe	1.01	1.26	1.29	1.00	0.91	0.99	Fe	1.05	1.35	0.90	1.22	0.86	0.83
Mn	0.02	0.01	0.01	0.01	0.01	0.01	Mn	0.01	0.03	0.01	0.02	0.01	0.01
Ca	0.00	0.01	0.02	0.01	0.01	0.01	Ca	0.02	0.00	0.01	0.00	0.01	0.01
K	0.75	0.69	0.48	0.61	0.69	0.65	K	0.60	0.32	0.65	0.51	0.78	0.67
Na	0.02	0.03	0.03	0.05	0.01	0.01	Na	0.03	0.00	0.04	0.04	0.02	0.03
Ti	0.14	0.15	0.07	0.08	0.08	0.08	Ti	0.08	0.15	0.09	0.11	0.08	0.09
Mg number Mg/(Mg + Fe) x 100													
	50.3	41.8	47.2	52.6	54.5	52.8		51.9	50.7	54.3	49.3	57.3	58.5

bdl=below detection limit

Table 20. Chlorite microprobe analyses for Portland brownstone.

	PB2			PB6				PB7			PB8		
	1	2	3	1	2	3		1	2	1	2	3	
SiO₂	26.67	22.94	21.60	25.50	24.09	23.98	SiO₂	24.90	23.91	23.67	24.48	24.82	
Al₂O₃	21.49	21.86	20.40	20.63	22.85	21.74	Al₂O₃	20.21	22.24	22.55	20.32	19.08	
MgO	15.76	10.64	13.01	13.26	15.84	13.65	MgO	14.23	14.51	15.37	13.43	19.45	
FeO	21.59	30.24	22.25	26.31	23.13	25.87	FeO	22.78	24.28	23.31	24.40	17.98	
MnO	0.25	bdl	0.26	0.17	0.12	0.40	MnO	0.35	0.34	0.35	0.29	0.11	
CaO	0.03	0.03	0.03	bdl	bdl	bdl	CaO	0.05	bdl	bdl	0.08	bdl	
K₂O	0.71	bdl	bdl	bdl	bdl	bdl	K₂O	bdl	bdl	bdl	bdl	bdl	
Na₂O	bdl	bdl	bdl	bdl	0.06	bdl	Na₂O	0.07	0.05	bdl	bdl	0.06	
TiO₂	0.28	0.20	0.07	0.11	bdl	bdl	TiO₂	0.07	0.09	0.07	0.10	0.09	
Total	86.80	85.91	77.63	85.99	86.08	85.64	Total	82.67	85.41	85.32	83.10	81.59	
Number of ions based on 28 O													
Si	5.57	5.10	5.14	5.51	5.12	5.22	Si	5.52	5.17	5.10	5.45	5.44	
Al	5.29	5.72	5.72	5.26	5.73	5.57	Al	5.28	5.67	5.72	5.33	4.93	
Mg	4.91	3.52	4.62	4.27	5.02	4.43	Mg	4.70	4.68	4.93	4.46	6.36	
Fe	3.77	5.62	4.43	4.76	4.11	4.71	Fe	4.22	4.39	4.20	4.54	3.30	
Mn	0.05	0.00	0.05	0.03	0.02	0.07	Mn	0.07	0.06	0.06	0.05	0.02	
Ca	0.01	0.01	0.01	0.00	0.00	0.00	Ca	0.01	0.00	0.00	0.02	0.00	
K	0.19	0.00	0.00	0.00	0.00	0.00	K	0.00	0.00	0.00	0.00	0.00	
Na	0.00	0.00	0.00	0.00	0.02	0.00	Na	0.03	0.02	0.00	0.00	0.02	
Ti	0.04	0.03	0.01	0.02	0.00	0.00	Ti	0.01	0.01	0.01	0.02	0.02	
Mg number Mg/(Mg + Fe) x 100													
	56.6	38.5	51.0	47.3	55.0	48.5		52.7	51.6	54.0	49.5	65.9	

bdl=below detection limit

Cement and Matrix

Portland brownstone is primarily cemented by quartz and albite. Lesser amounts of calcite and hematite cement are present (Fig. 26). There is also a significant amount of hematite in the matrix of the sandstone, contributing to the characteristic reddish brown color of Portland brownstone.

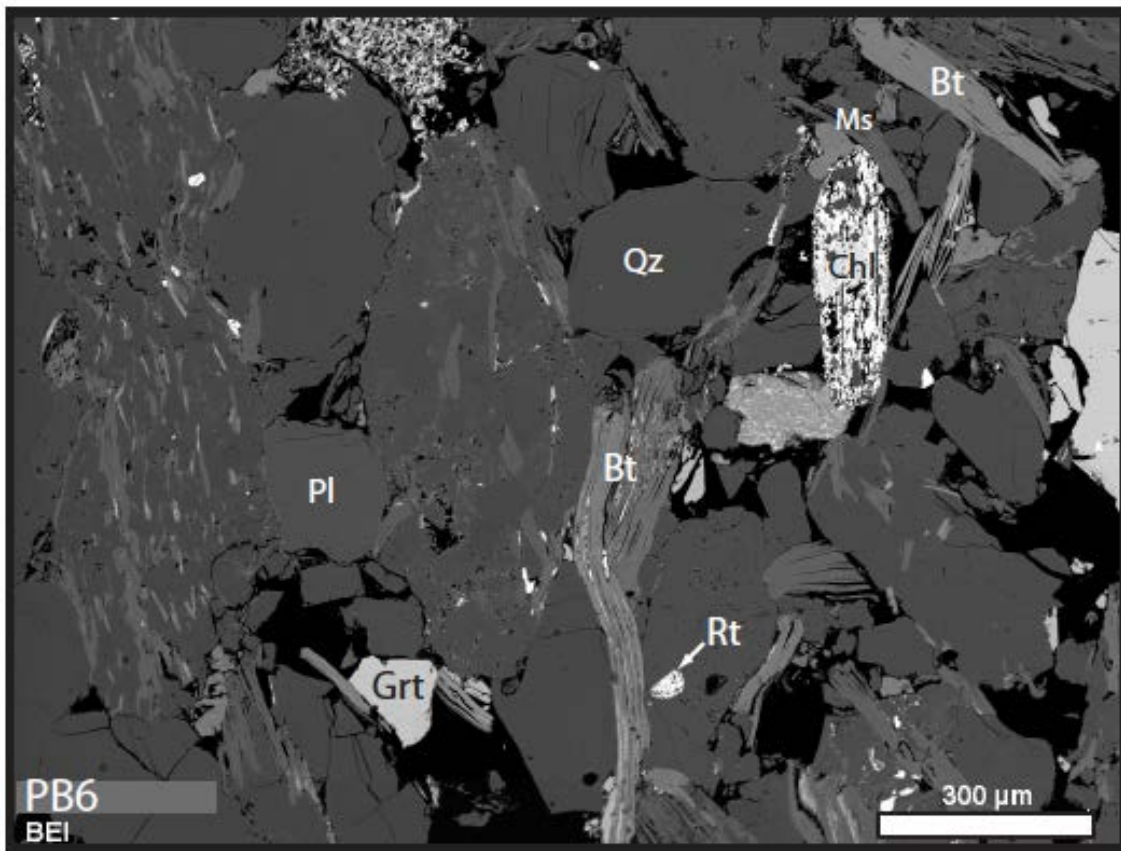


Figure 25. Backscatter image showing the accessory minerals garnet, rutile, biotite, muscovite, and chlorite in Portland brownstone. See Tables 2, 3, and 4 for abbreviations.

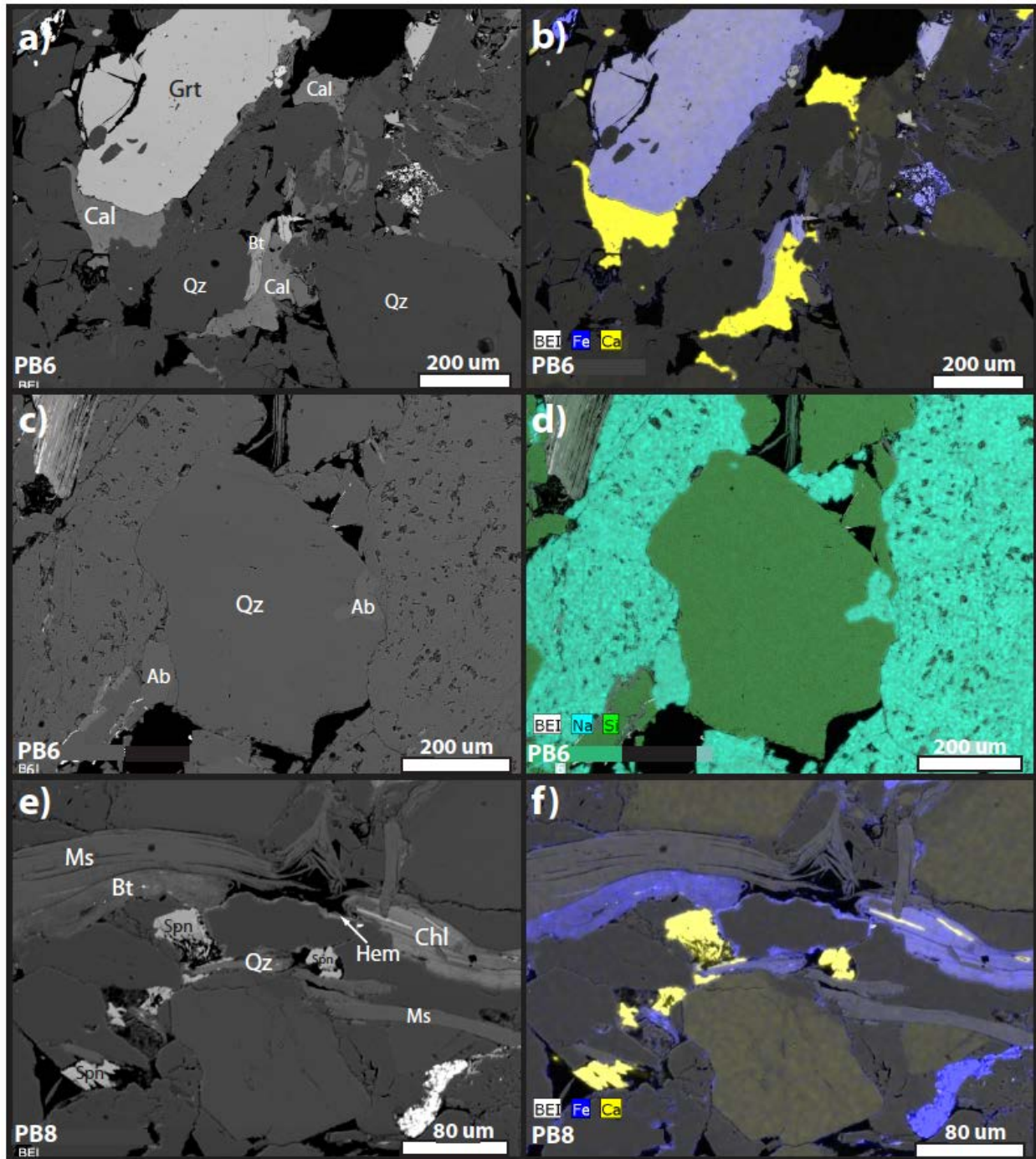


Figure 26. Mineralogy of cement in sample PB6 of Portland brownstone, (a) Backscatter image and (b) calcium element map (yellow) showing calcite cementing garnet and quartz, (c) Backscatter image and (d) sodium element map (aqua) showing albite cementing a quartz grain, (e) Backscatter image and (f) iron element map (blue) showing hematite cementing quartz. See Tables 2, 3, and 4 for abbreviations.

Stanford sandstone

Clastic Grains

Potassium and plagioclase feldspars were analyzed in the Stanford feldspathic arenite (Tables 21, 22a, and 22b). Feldspars make up 32-56% framework grains (Table 5). Microprobe analyses show potassium feldspar of composition ($\text{Ab}_{6-11}, \text{An}_0, \text{Or}_{88-93}$). In contrast to the other sandstones in this study, the Stanford sandstone contains only oligoclase ($\text{Ab}_{71-87}, \text{An}_{12-26}, \text{Or}_{0-4}$). Zoned feldspar was not found in these samples.

Muscovite and biotite occur in the Stanford sandstone (Tables 23 and 24). No chlorite was present in the samples analyzed for this study. Only one grain of muscovite was analyzed because the majority of muscovite grains were too small to obtain an analysis, and limited to small flakes within the matrix and crushed around grains. The muscovite analysis contained detectable levels of magnesium and iron. Potassium content in muscovite grain was routinely less (0.82 apfu) than the stoichiometric 1 K apfu.

Eight biotite analyses were done on the Stanford sandstone. Biotite grains were heavily oxidized and flakes were small, making it a challenge to target grains for analysis. All of the biotite analyses contain comparable amounts of iron and magnesium. Potassium contents in the biotite were low, routinely less (0.46 to 0.71 apfu) than the stoichiometric 1K apfu.

Accessory Minerals

Like with the Kulen Mountain sandstone and Portland brownstone, EDS reconnaissance confirmed the presence of accessory minerals in the Stanford sandstone. Stanford sandstone contains minimal amounts of zircon, apatite, and sphene (Figure 27). Zircon is the most abundant of these phases, and is extremely resistant to weathering (Taylor and Eggleton, 2001).

Table 21. Potassium feldspar microprobe analyses for Stanford sandstone.

	SU1	SU3	SU5	SU7	SU8
	4	2	1	2	2
SiO₂	64.91	65.48	64.81	65.72	65.42
TiO₂	0.05	bdl	0.08	bdl	bdl
Al₂O₃	18.24	18.49	18.28	18.23	18.15
FeO	bdl	bdl	0.07	0.08	0.19
MnO	bdl	bdl	bdl	bdl	bdl
MgO	bdl	bdl	bdl	bdl	bdl
CaO	bdl	bdl	bdl	bdl	bdl
Na₂O	0.84	1.24	0.68	0.74	0.84
K₂O	15.11	14.62	16.04	16.15	15.92
Total	99.14	99.82	99.96	100.92	100.52
Numbers of ions based on 8 O					
Si	3.01	3.01	3.00	3.01	3.01
Ti	0.00	0.00	0.00	0.00	0.00
Al	1.00	1.00	1.00	0.98	0.98
Fe	0.00	0.00	0.00	0.00	0.01
Mn	0.00	0.00	0.00	0.00	0.00
Mg	0.00	0.00	0.00	0.00	0.00
Ca	0.00	0.00	0.00	0.00	0.00
Na	0.08	0.11	0.06	0.07	0.08
K	0.89	0.86	0.95	0.94	0.93
Mol per cent end-members					
Ab	7.8	11.4	6.0	6.5	7.5
An	0.0	0.0	0.0	0.0	0.0
Or	92.2	88.6	94.0	93.5	92.5

bdl=below detection limit

Table 22a. Plagioclase feldspar microprobe analyses for Stanford sandstone.

	SU1				SU3		
	3	4	5	6	1	2	3
SiO₂	63.96	62.28	61.76	61.46	62.77	66.22	63.01
TiO₂	bdl	0.08	bdl	bdl	bdl	bdl	bdl
Al₂O₃	21.44	22.75	22.78	22.99	22.28	21.50	23.85
FeO	0.12	0.18	0.13	0.16	0.20	0.07	0.17
MnO	bdl	bdl	bdl	bdl	bdl	bdl	bdl
MgO	bdl	bdl	bdl	bdl	bdl	bdl	bdl
CaO	3.19	4.79	4.84	5.05	3.80	2.59	5.04
Na₂O	9.33	8.52	8.33	8.18	8.67	10.03	7.83
K₂O	0.35	0.27	0.36	0.29	0.66	0.08	0.50
Total	98.39	98.87	98.20	98.12	98.39	100.49	100.39
Numbers of ions based on 8 O							
Si	2.86	2.79	2.79	2.77	2.82	2.89	2.78
Ti	0.00	0.00	0.00	0.00	0.00	0.00	0.00
Al	1.13	1.20	1.21	1.22	1.18	1.11	1.24
Fe	0.00	0.01	0.00	0.01	0.01	0.00	0.01
Mn	0.00	0.00	0.00	0.00	0.00	0.00	0.00
Mg	0.00	0.00	0.00	0.00	0.00	0.00	0.00
Ca	0.15	0.23	0.23	0.24	0.18	0.12	0.24
Na	0.81	0.74	0.73	0.72	0.76	0.85	0.67
K	0.02	0.02	0.02	0.02	0.04	0.00	0.03
Mol per cent end-members							
Ab	82.4	75.1	74.1	73.2	77.4	87.1	71.5
An	15.6	23.3	23.8	25.0	18.7	12.4	25.4
Or	2.0	1.6	2.1	1.7	3.9	0.5	3.0

bdl=below detection limit

Table 22b. Plagioclase feldspar microprobe analyses for Stanford sandstone.

	SU5			SU7		SU8		
	1	2	3	1	3	1	2	3
SiO₂	63.10	67.87	62.31	62.65	62.50	64.64	64.74	63.09
TiO₂	bdl	bdl	bdl	bdl	bdl	bdl	0.04	bdl
Al₂O₃	23.50	21.00	22.83	23.72	23.18	22.05	22.76	23.56
FeO	0.10	0.08	0.15	0.11	bdl	0.13	bdl	0.26
MnO	bdl	bdl	bdl	bdl	bdl	bdl	bdl	bdl
MgO	bdl	bdl	bdl	bdl	bdl	0.03	bdl	bdl
CaO	5.51	3.27	4.29	5.38	5.06	3.77	4.41	5.37
Na₂O	8.32	8.95	8.97	8.22	8.65	8.90	8.77	8.18
K₂O	0.20	0.08	0.17	0.14	0.36	0.25	0.25	0.23
Total	100.73	101.27	98.72	100.21	99.75	99.78	100.97	100.69
Numbers of ions based on 8 O								
Si	2.77	2.93	2.79	2.77	2.78	2.85	2.83	2.77
Ti	0.00	0.00	0.00	0.00	0.00	0.00	0.00	0.00
Al	1.22	1.07	1.21	1.23	1.21	1.15	1.17	1.22
Fe	0.00	0.00	0.01	0.00	0.00	0.00	0.00	0.01
Mn	0.00	0.00	0.00	0.00	0.00	0.00	0.00	0.00
Mg	0.00	0.00	0.00	0.00	0.00	0.00	0.00	0.00
Ca	0.26	0.15	0.21	0.25	0.24	0.18	0.21	0.25
Na	0.71	0.75	0.78	0.70	0.75	0.76	0.74	0.70
K	0.01	0.00	0.01	0.01	0.02	0.01	0.01	0.01
Mol per cent end-members								
Ab	72.4	82.8	78.3	72.8	74.0	79.8	77.1	72.4
An	26.5	16.7	20.7	26.3	23.9	18.7	21.4	26.3
Or	1.1	0.5	1.0	0.8	2.1	1.5	1.4	1.3

bdl=below detection limit

Table 23. Muscovite microprobe analysis for Stanford sandstone.

SU1	
1	
SiO₂	43.67
Al₂O₃	36.22
MgO	0.51
FeO	0.81
MnO	bdl
CaO	bdl
K₂O	10.28
Na₂O	0.43
TiO₂	0.52
Total	92.44
Numbers of ions based on 10 O	
Si	2.72
Al	2.66
Mg	0.05
Fe	0.04
Mn	0.00
Ca	0.00
K	0.82
Na	0.05
Ti	0.02

bdl=below detection limit

Table 24. Biotite microprobe analyses for Stanford sandstone.

	SU1			SU8				
	1	2	3	1	2	3	4	5
SiO₂	37.02	36.99	34.96	40.02	38.87	51.10	42.07	41.92
Al₂O₃	15.52	15.37	14.53	9.95	13.42	18.57	16.58	16.30
MgO	9.96	8.63	8.70	5.53	10.34	4.21	8.14	7.91
FeO	15.63	17.63	18.20	15.38	13.48	10.73	13.78	14.64
MnO	0.17	0.31	bdl	0.10	0.27	bdl	0.08	0.21
CaO	0.12	0.26	0.22	0.15	0.31	0.48	0.21	0.24
K₂O	7.77	7.71	6.98	6.28	6.28	5.74	6.31	5.67
Na₂O	0.05	0.24	0.06	0.12	0.34	0.26	0.15	0.19
TiO₂	3.49	2.18	3.81	3.35	3.65	1.90	3.12	1.73
Total	89.72	89.31	87.45	80.88	86.95	93.01	90.43	88.81
Number of ions based on 10 O								
Si	2.65	2.69	2.60	3.12	2.81	3.24	2.88	2.92
Al	1.31	1.32	1.28	0.92	1.14	1.39	1.34	1.34
Mg	1.06	0.93	0.97	0.64	1.11	0.40	0.83	0.82
Fe	0.93	1.07	1.13	1.00	0.81	0.57	0.79	0.85
Mn	0.01	0.02	0.00	0.01	0.02	0.00	0.00	0.01
Ca	0.01	0.02	0.02	0.01	0.02	0.03	0.02	0.02
K	0.71	0.71	0.66	0.63	0.58	0.46	0.55	0.50
Na	0.01	0.03	0.01	0.02	0.05	0.03	0.02	0.03
Ti	0.19	0.12	0.21	0.20	0.20	0.09	0.16	0.09
Mg number Mg/(Mg + Fe) x 100								
	53.2	46.6	46.0	39.0	57.8	41.2	51.3	49.1

bdl=below detection limit

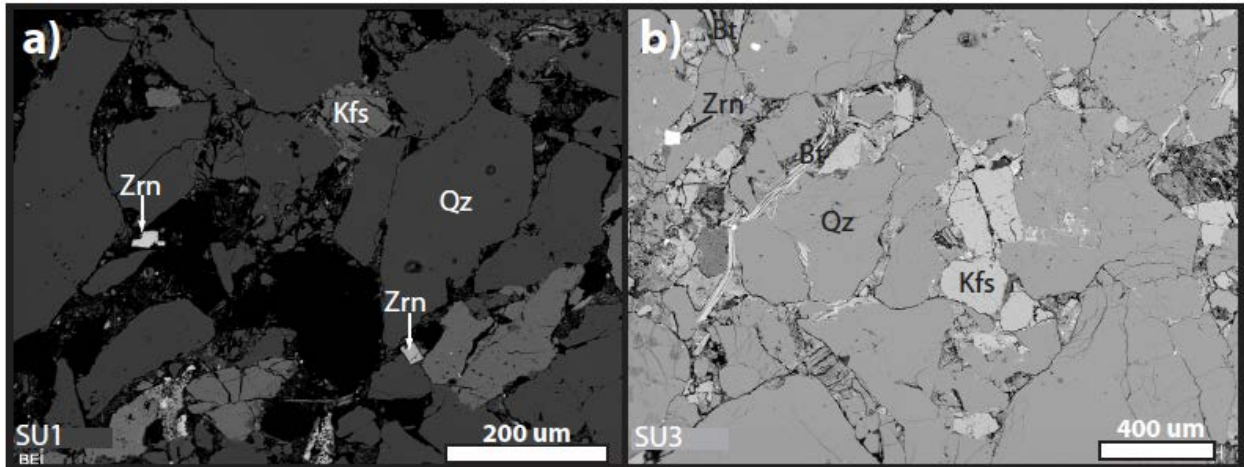


Figure 27. Backscatter image showing accessory minerals (a) zircon and (b) biotite in Stanford sandstone. For abbreviations see Tables 2, 3, and 4.

Cement and Matrix

The Stanford sandstone does not contain abundant cement. Cement present is hematite, goethite, and albite (Figure 28). The matrix of the sandstone is rich in iron, which can explain the characteristic tan color of the weathered sandstone. Additionally, element mapping reveals that the matrix of the Stanford sandstone contains high levels of magnesium (Figure 29). The presence of magnesium can be attributed to magnesium-rich smectite.

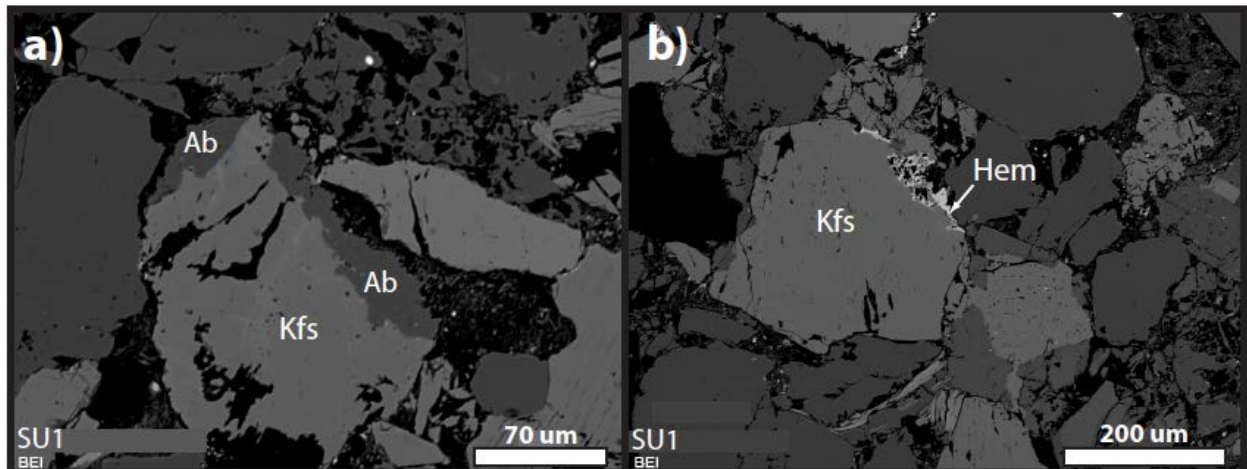


Figure 28. Cement in Stanford sandstone. (a) albite cementing potassium feldspar and (b) hematite cementing potassium feldspar. For abbreviations see Tables 2, 3, and 4.

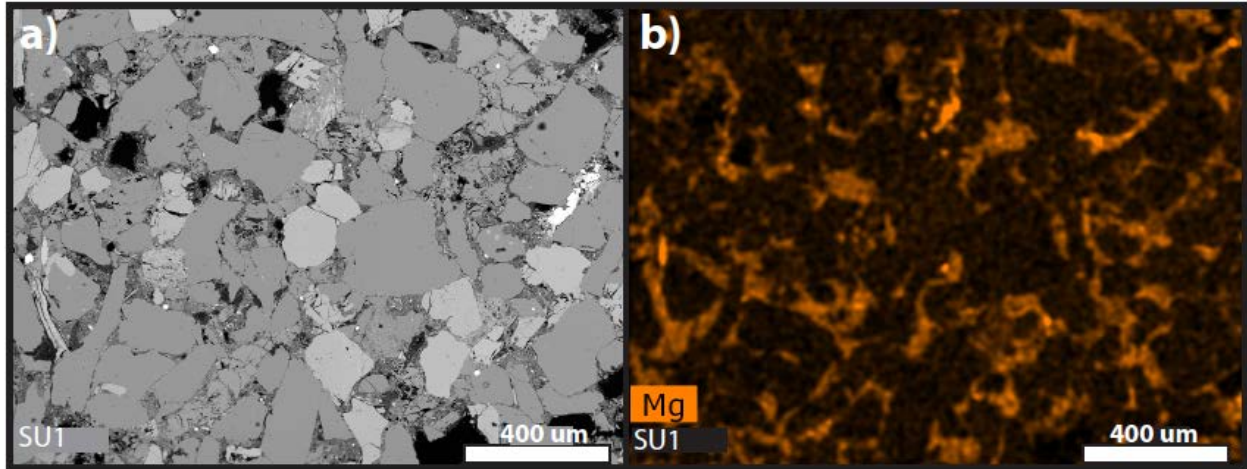


Figure 29. (a) Backscatter image and (b) element map of Stanford sandstone showing a magnesium rich matrix (orange).

DISCUSSION AND CONCLUSIONS

The sandstone quarry presents a unique situation in the discussion of sandstone weathering because in the strict sense the exposure of the sandstone is not completely natural, but it also is not weathering in the built environment. Consider that in a quarry, stone is exploited perpendicular to horizontal bedding surfaces and left exposed immediately. In a completely natural setting, sandstone weathers by gradual exposure to water in soil, eventually disaggregating into soil. The classical soil profile is the expression of natural weathering. In the built environment, weathering of sandstone is accelerated by a variety of factors including the building drainage system, presence or absence of mortar, and the orientation of the stone in the building.

Although weathering conditions in a quarry vary from a completely natural setting, it is still useful to consider the acronym for soil-forming factors to aid in this comparison. CLORPT stands for climate, organics, relief, parent material, and time (Garrison, 2003). This acronym can be adapted to looking at sandstone by using it as the “parent material” and assessing the effects of climate, biological growth, relief, and time on the mineralogy of the framework grains, accessory minerals, matrix, cement, and clay fraction that make up the sandstone.

Weathering of the Masonry Sandstones

Kulen Mountain sandstone

The Angkor temples and Kulen Mountain quarries are located in the humid, tropical monsoon climate of Cambodia. Heavy vegetation and large quantities of precipitation during the rainy season characterize this climate. Deforested areas experience large variation in diurnal temperature during the dry season. Vegetation shields the sandstone from diurnal temperature changes in the dry season, but also create a “crust” on the sandstone from biological colonization on the surface. The buildings locally host bat populations and guano that contributes to the weathering of the sandstone.

Kulen Mountain sandstone is a fine to medium grained, moderately well-sorted feldspathic arenite cemented by calcite and chlorite. It contains chlorite, mixed chlorite-smectite, mica-illite, and calcite in the clay fraction. Quarry material examined in this study does not contain kaolinite in the clay fraction. Oxidation of mica and chlorite and leaching of potassium occurs in all samples, indicating a strong degree of weathering. The weathering of clastic grains happens both before and after sandstone formation.

Under the petrographic microscope, the grey sandstone quarry samples appear similar based on mineralogy, sorting, grain size, and cement. Further examination with the electron microprobe, however, revealed that the matrix and clay fraction vary from sample to sample. EDS elemental mapping showed that the matrix of sample 109B contained mostly calcite, while sample 104B contains almost no calcite. Samples 109M and 109B have calcite and a higher proportion of smectite in the mixed chlorite-smectite in the clay fraction, in addition to the chlorite and mica-illite found in the remainder of the samples.

Most of the weathering observed in the temples ties to areas with poor drainage, particularly column bases, platform surfaces, and the ceilings of galleries (Table 25). Poor drainage poses great concern during the monsoon season because of wetting-drying cycles, and constant re-wetting from standing water. Salt crystallization related to bat guano and biological crusts are exacerbated by constant re-wetting. With these primary concerns in mind, stone conservators should not be treating all the “grey sandstone” of the temples alike. The EDS and XRD results show that they will behave quite differently, especially under circumstances where wetting-drying cycles occur.

Samples with a matrix of calcite and containing smectite in the clay fraction behave poorly if wetted (Table 25). Calcite readily dissolves. The dissolved calcium of samples 109M and 109B would contribute to the precipitation of calcium salts as observed by Hosono et al. (2006). The more chlorite-rich variety of the grey sandstone would be less susceptible to this type of disaggregation since its matrix is not filled with calcite. Samples 109M and 109B are also the most susceptible to swelling and shrinking from wetting-drying cycles because they contain more smectite. These samples are less weathered than the more chlorite-rich 109T, and are located lower stratigraphically on the outcrop.

Table 25. Summary of building weathering features.

Locality	Climate	Detrital Minerals*	Intergranular Minerals	Building Weathering Features	Possible Causes
Kulen Mountain, Cambodia	Humid tropical	Muscovite, Biotite, Chlorite, Garnet, Epidote, Rutile, Ilmenite, Magnetite, Xenotime, Sphene, Zeolite, Apatite	Chlorite-Smectite, Calcite, Illite, Mica, Goethite	Contour scaling	Wetting-Drying
				Exfoliation/Delamination	Wetting-Drying
				Case hardening	Wetting-Drying
				Salt crystallization	Dissolution of minerals within the sandstone matrix and recrystallization as salts; Salts formed from bat droppings
				Biological colonization	Vegetation traps moisture next to the stone, allowing the formation of biological crust
Portland, Connecticut	Humid temperate	Muscovite, Biotite, Chlorite, Garnet, Apatite, Amphibole, Ilmenite, Magnetite, Sphene	Chlorite-Smectite, Illite, Mica, Hematite	Contour scaling	Wetting-drying Freeze-thaw
				Exfoliation/Delamination	Wetting-drying Freeze-thaw Face-bedding
				Cryptoflorescence	Wetting-drying Incompatible patching material
				Biological colonization	Prolonged wetting of stone surface
Stanford, California	Mediterranean	Muscovite, Biotite, Glauconite, Zircon, Apatite, Rutile	Illite-Smectite, Kaolinite, Illite, Mica, Goethite	Efflorescence	Wetting-drying
				Biological colonization	Prolonged wetting of stone surface
				Case hardening	Wetting-drying Incompatible patching material

*Detrital minerals also include the framework grains feldspar and quartz for all samples.

Portland brownstone

The Portland brownstone quarries, located in the northeastern United States, are located in a temperate climate, meaning they experience cold, snowy winters and mild summers. Average precipitation is about 1160 mm per year (average from 1901-2000), with the wettest seasons occurring during the spring and fall. Temperatures cycle above and below freezing during the winter months (National Climatic Data Center Time Series, 2015). The humid climate contributes to the weathering of the sandstone.

Portland brownstone is a medium to coarse grained, poorly sorted, plagioclase-rich feldspathic arenite cemented by albite, quartz, and calcite, with hematite acting as secondary cement. Clay fraction analysis reveals the absence of swelling clays in Portland brownstone with the exception of a small amount of chlorite-smectite, as both chlorite and illite are non-swelling. The Portland Formation soil contains no expandable clays whatsoever. Although the small proportion of expandable smectite layers in the chlorite may contribute to damage through swelling and shrinking cycles, the lack of any other expandable clays suggests this is not the primary mechanism for the rapid weathering described in many nineteenth century buildings. Another contribution to building weathering is the leaching of alkalis from mica. Alkali leaching contributes to the formation of salts.

Contour scaling and cryptoflorescence account for much of the observed damage to Portland brownstone structures in New England and New York (Table 25). Trapped moisture causes swelling and salt migration, particularly in areas with poor drainage and surfaces covered with stucco or paint. Further damage is imposed through freeze-thaw cycles. Mortar and patching compatibility are significant because this material must have an expansion coefficient similar to that of the stone to ensure that freeze-thaw cycles will not cause cracking of the

sandstone. Additionally, incompatible mortar and patching materials can exacerbate problems with ion leaching and subsequent salt formation (Jiménez González et al., 2012). Because of the laminated structure of sandstone, another important factor to consider is the orientation of the sandstone block within the building. Delamination occurs if the block is laid face-bedded.

Deterioration can plausibly be tied to two factors in the natural weathering profile. One is that Portland brownstone is poorly sorted, has variable grain size on even the order of a thin section or hand sample, and is poorly cemented in places. The porosity changes with weathering. Clay migrates when wetted and significantly reduces the permeability of the sandstone. Even small amounts of mixed layered clays with expandable layers contribute to this phenomena (Gray and Rex, 1966). In the event moisture gets trapped, and undergoes a freeze-thaw cycle or the crystallization of salts, the sandstone disaggregates under the crystallization pressure. Over time, when brownstone was in peak demand, the use of poorer quality stone would add to the problem. Another factor that contributes to deterioration lies with the incompatibility of adjacent materials. Mortar, stucco, patching materials, and paint are all affected by leaching alkalis and salt crystallization.

Stanford sandstone

Stanford and the source of the Stanford sandstone, the former Greystone Quarry, are located in a semiarid Mediterranean climate. Mediterranean climates are characterized by warm, dry summers and cool winters. Most precipitation falls during the winter months, averaging 500 mm annually. Average winter temperatures are around 9°C, and rarely fall below freezing (National Climatic Data Center Time Series, 2015).

Stanford sandstone is a fine to medium-grained, moderately well-sorted feldspathic arenite cemented by quartz, goethite, albite, and hematite. This sandstone contains a small

quantity of accessory minerals, and contains little mica. The Stanford sandstone contains volcanic lithic fragments with microphenocrysts of plagioclase feldspar. The volcanic clasts would be susceptible to weathering, indicating that Stanford sandstone is a less mature sandstone than either the Kulen Mountain sandstone or Portland brownstone. Stanford sandstone comes from an eroding magmatic arc. In contrast, Kulen Mountain sandstone and Portland brownstone come from a terrain of regional metamorphic rock and an eroded orogen. Clay fraction analysis shows the presence of mixed illite-smectite and kaolinite in the Stanford sandstone. Smectite exhibits swelling behavior, while illite and kaolinite are typically non-swelling clays.

In many places, the sandstone of the Stanford Main Quad maintains excellent preservation, likely accounted for by the overall dryness of the climate. The intricate carvings on the entrance archway to Memorial Church are one example of this high level of preservation. However, other areas, particularly column bases, blocks at the base of buildings, and cornices present symptoms such as flaking, case hardening, efflorescence, and biological colonization.

These problems seem to relate most to poor drainage management and incompatible patching materials (Table 25). The presence of smectite in the clay fraction means that architectural elements vulnerable to consistent water exposure likely experience swelling and loss of tensile strength. Given the presence of kaolinite and the lack of a sizeable amount of mica, it is probable that the feldspars and lithic volcanic fragments contribute the most to weathering. The biological colonization found on much of the Stanford sandstone can also be attributed to poor drainage.

IMPLICATIONS FOR HISTORIC PRESERVATION

Kulen Mountain Sandstone

The mineralogy of the Kulen Mountain sandstone varies widely at the individual outcrop scale. Calcite and swelling clays in the matrix of some of the Kulen Mountain sandstone make it particularly vulnerable to damage from water. The distribution of the sandstone containing calcite and swelling clays should be characterized in order to determine the areas of the temples most at risk for water damage and salt crystallization, and plan for any future chemical treatment of the stone during conservation.

Portland Brownstone

The absence of swelling clays in the Portland brownstone suggests that other mechanisms are responsible for the swelling. This exact mechanism remains unknown. Distribution of clay in the pore structure is one avenue that should be explored. Additionally, the presence of calcite cement is problematic because of the potential for calcite dissolution and reprecipitation as salts. Portland brownstone should be kept dry and not laid face-bedded in order to preserve it because once the cement breaks down, restoration efforts will not be practical.

Stanford Sandstone

The most pressing concern for preservation of the Stanford sandstone is protection from water. Swelling smectite layers in the illite-smectite of the clay fraction and poor cementation make the Stanford sandstone susceptible to wetting damage. The lack of calcite cement in these weathered samples compared to calcite reported by previous authors suggests that the calcite has weathered away. Finally, oxidation poses no concern for preservation because the characteristic tan color and occasional red banding in the sandstone appears to have occurred prior to when the sandstone was quarried.

REFERENCES

- Adamovic, J., 2005, Sandstone cementation and its geomorphic and hydraulic implication: *Ferrantia*, v. 44, p. 21-24.
- André, M.-F., Etienne, S., Mercier, D., Vautier, F., and Voldoire, O., 2008, Assessment of sandstone deterioration at Ta Keo temple (Angkor): first results and future prospects: *Environmental Geology*, v. 56, no. Special Issue "Monument Future: climate change, air pollution, decay and conservation", p. 677-688.
- André, M.-F., Phalip, B., Voldoire, O., Vautier, F., Géraud, Y., Benbakkar, M., Constantin, C., Huber, F., and Morvan, G., 2011, Weathering of sandstone lotus petals at the Angkor site: a 1,000-year stone durability trial: *Environmental Earth Science*, v. 63, no. Special Issue "Monuments Under Threat: Environmental Impact and Preservation Strategies", p. 1723-1739.
- André, M.-F., Voldoire, O., Roussel, E., Vautier, F., Phalip, B., and Peou, H., 2012, Contrasting weathering and climate regimes in forested and cleared sandstone temples of the Angkor region: *Earth Surface Processes and Landforms*, v. 37, p. 519-532.
- April, R. H., 1981, Clay Petrology of the Upper Triassic/Lower Jurassic Terrestrial Strata of the Newark Supergroup, Connecticut Valley, U.S.A.: *Sedimentary Geology*, v. 29, p. 283-307.
- Architectural Resources Group, 1988, Stanford University: Main Quad Stone Restoration Study: Architectural Resources Group.
- Banfield, J. F., and Eggleton, R. A., 1990, Analytical transmission electron microscope studies of plagioclase, muscovite, and k-feldspar weathering: *Clays and Clay Minerals*, v. 38, no. 1, p. 77-89.
- Bisdom, E. G. A., Stoops, G., Delvigne, J., Curmi, P., and Atlemuller, H.-J., 1982, Micromorphology of weathering biotite and its secondary products: *Pedologie*, v. 32, no. 2, p. 225-252.
- Blatt, H., and Tracy, R. J., 1996, *Petrology: Igneous, Sedimentary, and Metamorphic*, New York, W.H. Freeman and Co.
- Brufau, A., and Vicente, M. A., 1986, Weathering of the Villamayor arkosic sandstone used in buildings, under a continental semi-arid climate: *Applied Clay Science*, v. 1, p. 265-272.
- Building & Monument Conservation, 2012, *Brownstone & Masonry Repairs and Exterior Historic Structures Report: Concord Town House*.

- Buurman, P., Meijer, E. L., and van Wijck, J. H., 1988, Weathering of chlorite and vermiculite in ultramafic rocks of Cabo Ortegal, Northwestern Spain: *Clays and Clay Minerals*, v. 36, no. 3, p. 263-269.
- California Geological Survey, 2006, Simplified Geologic Map of California: Department of Conservation
- Camarasa-Belmonte, A. M., and Soriano, J., 2014, Empirical study of extreme rainfall intensity in a semi-arid environment at different time scales: *Journal of Arid Environments*, v. 100-101, p. 63-71.
- Carò, F., and Douglas, J. G., 2013, Nature and provenance of the sandstone used for Bayon style sculptures produced during the reign of Jayavarman VII: *Journal of Archaeological Science*, v. 40, no. 1, p. 723-734.
- Carò, F., Douglas, J. G., and IM, S., 2010, Towards a Quantitative Petrographic Database of Khmer Stone Materials- Koh Ker Style Sculpture: *Archaeometry*, v. 2, p. 191-208.
- Carò, F., and IM, S., 2012, Khmer sandstone quarries of Kulen Mountain and Koh Ker: a petrographic and geochemical study: *Journal of Archaeological Science*, v. 39, p. 1455-1466.
- Critelli, S., and Nilsen, T. H., 1996, Petrology and Diagenesis of the Eocene Butano Sandstone, La Honda Basin, California: *The Journal of Geology*, v. 104, no. 3, p. 295-315.
- Dagens, B., 2002, History of the Angkor Site: *Museum International*, v. 54, no. 1 & 2, p. 12-22.
- Delvert, J., 1963, Recherches sur l' <<érosion>> des grès des monuments d'Angkor: *Bulletin de l'Ecole française d'Extrême-Orient*, v. 51, no. 2, p. 453-534.
- Doehne, E., and Price, C. A., 2010, *Stone Conservation: An Overview of Current Research*, in Institute, T. G. C., ed.: Los Angeles, Getty Publications.
- Dott, R. H., 1964, Wacke, graywacke and matrix- What approach to immature sandstone classification?: *Journal of Sedimentary Petrology*, v. 34, no. 3, p. 625-632.
- French, L., 1999, Hierarchies of Value at Angkor Wat: *Ethnos*, v. 62, no. 2, p. 170-191.
- Garrison, E., 2003, *Techniques in Archaeological Geology*, Springer, Natural Science in Archaeology.
- Glossary of Geology, 2011, in Neuendorf, K. K. E., Mehl, J. P., and Jackson, J. A., eds.: Alexandria, VA, American Geosciences Institute.
- Google Maps, 2015, Sampling location map of Stanford sandstone: Google Maps.
- Gray, D. H., and Rex, R. W., 1966, Formation damage in sandstones caused by clay dispersion and migration: *Clays and Clay Minerals*, 14th National Conference, v. 26, p. 355-366.

- Guinness, A. C., 2003, Heart of Stone: The Brownstone Industry of Portland, Connecticut, *in* LeTourneau, P. M., and Olsen, P. E., eds., *The Great Rift Valleys of Pangea in Eastern North America, Volume 2*: New York, Columbia University Press, p. 224-247.
- Hale, P. A., and Shakoor, A., 2003, A Laboratory Investigation of the Effects of Cyclic Heating and Cooling, Wetting and Drying, and Freezing and Thawing on the Compressive Strength of Selected Sandstones: *Environmental and Engineering Geoscience*, v. 9, no. 2, p. 117-130.
- Harkin, B., 2012, Brownstones on Berkeley Place in Park Slope, Brooklyn: Bidding Farewell to a City's Precious Stone, *New York Times*.
- Harris, E. A., 2012, Bidding Farewell to a City's Precious Stone, *The New York Times*: New York City, *The New York Times*.
- Highsmith, C. M., 1980, The Pacific-Union Club in the former James C. Flood mansion, *Library of Congress*.
- Hosono, T., Uchida, E., Suda, C., Ueno, A., and Nakagawa, T., 2006, Salt weathering of sandstone at the Angkor monuments, Cambodia: identification of the origins of salts using sulfur and strontium isotopes: *Journal of Archaeological Science*, v. 33, p. 1541-1551.
- Hubert, J. F., Feshbach-Meriney, P. E., and Smith, M. A., 1992, The Triassic-Jurassic Hartford Rift Basin, Connecticut and Massachusetts: Evolution, Sandstone Diagenesis, and Hydrocarbon History: *AAPG Bulletin*, v. 76, no. 11, p. 1710-1734.
- Istok, J. D., and Harward, M. E., 1982, Influence of Soil Moisture on Smectite Formation in Soils Derived from Serpentinite: *Soil Science Society of America Journal*, v. 46, no. 5, p. 1106-1108.
- Jiménez González, I., Flatt, R., Wangler, T., and Scherer, G. W., 2012, Factors affecting Portland Brownstone durability: A review, *Saarbrücken, LAP Lambert* 119 p.:
- Joncas, R., Neuman, D. J., and Turner, P. V., 2006, *The Campus Guide: Stanford University*, *in* University, S., ed.: New York, Princeton Architectural Press.
- Junkerman, C., 2010, A Biography of Stanford Sandstone: From Greystone Quarry to *Stone River*, *Sandstone and Tile, Volume 34*: Stanford University, Stanford Historical Society, p. 3-16.
- LeTourneau, P. M., 1985, *The Sedimentology and Stratigraphy of the Lower Jurassic Portland Formation, Central Connecticut* [Master of Arts: Wesleyan University, 240 p.
- McLaughlin, R. J., and Clark, J. C., 2004, Stratigraphy and structure across the San Andreas Fault zone in the Loma Prieta region and deformation during the earthquake: *U.S. Geological Survey Professional Paper 1550-E*, p. 5-47.

- Meehan, M., 2011, Meeting, August 2011, Portland Brownstone Quarries, Inc.
- Moore, D. M., and Reynolds, R. C., 1997, X-Ray Diffraction and the Identification and Analysis of Clay Minerals, New York, Oxford University Press.
- National Climatic Data Center Time Series, 2015, National Oceanic and Atmospheric Administration.
- Pettijohn, F. J., 1941, Persistence of Heavy Minerals and Geologic Age: *Journal of Geology*, v. 49, no. 6, p. 610-625.
- Racey, A., Love, M. A., Canham, A. C., Goodall, J. G. S., Polachan, S., and Jones, P. D., 1996, Stratigraphy and Reservoir Potential of the Mesozoic Khorat Group, NE Thailand: *Journal of Petroleum Geology*, v. 19, no. 1, p. 5-40.
- Resor, P., and deBoer, J., 2005, Hartford Basin Cross Section- Southington to Portland CT: Department of Environmental Protection.
- Scherer, G. W., Flatt, R., and Wheeler, G., 2001, Materials Science Research for the Conservation of Sculpture and Monuments: *Materials Research Society Bulletin*, v. January.
- Sharman, G. R., Graham, S. A., Grove, M., Kimbrough, D. L., and Wright, J. E., 2014a, Detrital zircon provenance of the Late Cretaceous-Eocene California forearc: Influence of Laramide low-angle subduction on sediment dispersal and paleogeography: *GSA Bulletin*, v. 127, no. 1/2, p. 38-60.
- Sharman, G. R., Graham, S. A., Grove, M., Kimbrough, D. L., and Wright, J. E., 2014b, DR2014263, Detrital Detrital zircon provenance of the Late Cretaceous-Eocene California forearc: Influence of Laramide low-angle subduction on sediment dispersal and paleogeography , Supplementary Materials, *GSA Bulletin Data Repository*.
- Short, W. R., 1986, *Geology of the Santa Teresa Hills, Santa Clara County, California* [M.S.: California State University, 141 p.
- Siedel, H., Pfefferkorn, S., von Plehwe-Leisen, E., and Leisen, H., 2010, Sandstone weathering in tropical climate: Results of low-destructive investigations at the temple of Ankor Wat, Cambodia: *Engineering Geology*, v. 115, p. 182-192.
- Stanford University Map, 1965: Stanford University, SC1049_m1723_ca1965_recto.
- Taylor, G., and Eggleton, R. A., 2001, *Regolith Geology and Geomorphology*, Chichester, John Wiley & Sons.
- Turkington, A. V., and Paradise, T. R., 2005, Sandstone weathering: a century of research and innovation: *Geomorphology*, v. 67, p. 229-253.

Uchida, E., Ito, K., and Shimizu, N., 2010, Provenance of the Sandstone Used in the Construction of the Khmer Monuments in Thailand: *Archaeometry*, v. 52, no. 4, p. 550-574.

Uchida, E., Shimoda, I., Takubo, Y., and Toyouchi, K., 2012, Moisture content measurement and surface water absorption test in the inner gallery of Bayon for the conservation of the bas-relief: *Journal of Archaeological Science*, v. 39, p. 1420-1435.

van de Kamp, P. C., and Leake, B. E., 1996, Petrology, geochemistry, and Na metasomatism of Triassic-Jurassic non-marine clastic sediments in the Newark, Hartford, and Deerfield rift basins, northeastern USA: *Chemical Geology*, v. 133, p. 89-124.

Wangler, T., and Scherer, G. W., 2009, Clay swelling inhibition mechanism of α,ω -diaminoalkanes in Portland Brownstone: *Journal of Materials Research*, v. 24, no. 5, p. 1646-1652.

World Monuments Fund, 2012.